






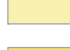

















APPENDIX B

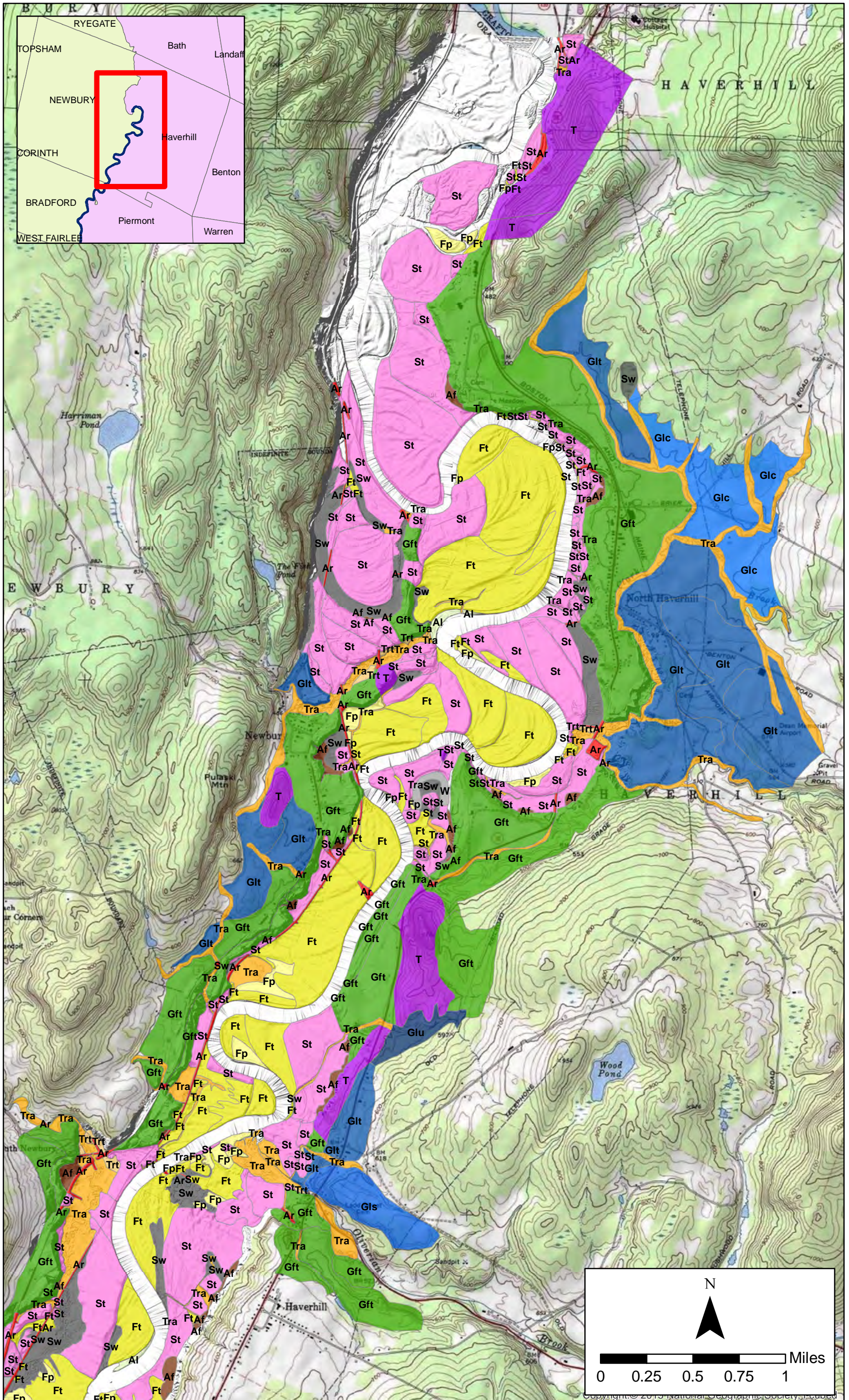
Surficial Geological Maps

[This page intentionally left blank.]

Map legend

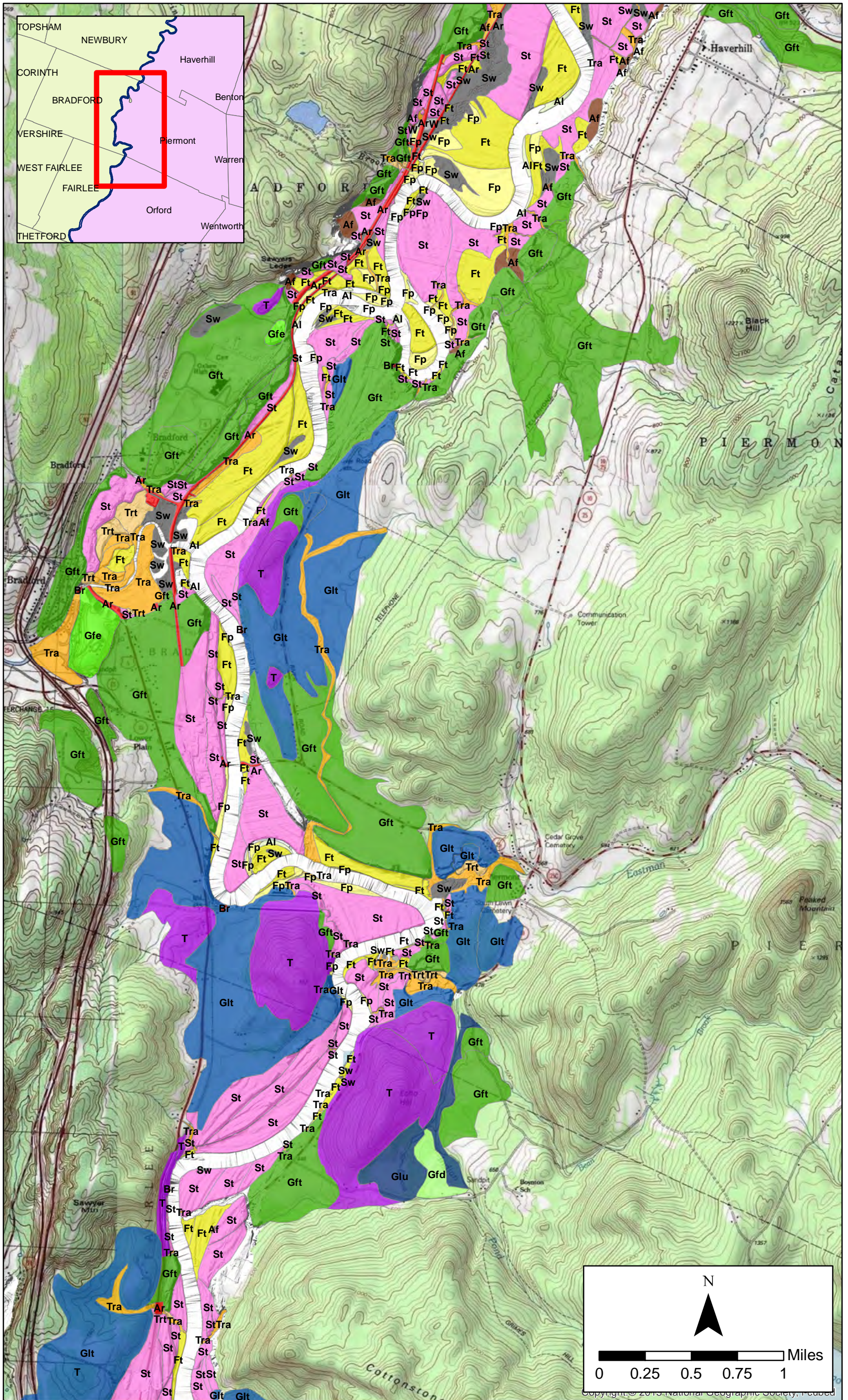
Surficial map units

	Alluvial fan (Af)
	Artificial fill (Ar)
	Bedrock (Br)
	Channel alluvium (Al)
	Eolian deposits (Eo)
	Floodplain (Fp)
	Flood terrace (Ft)
	Glaciofluvial deposit (Gfd)
	Glaciofluvial esker (Gfe)
	Glaciofluvial terrace (Gft)
	Glaciolacustrine clay (Glc)
	Glaciolacustrine sand (Gls)
	Glaciolacustrine terrace (Glt)
	Glaciolacustrine undifferentiated (Glu)
	Stream terrace (St)
	Stream terrace high (Sth)
	Stream terrace low (Stl)
	Till (T)
	Thin till (Tt)
	Tributary alluvium (Tra)
	Tributary stream terrace (Trt)
	Swamp deposits (Sw)
	Water (W)



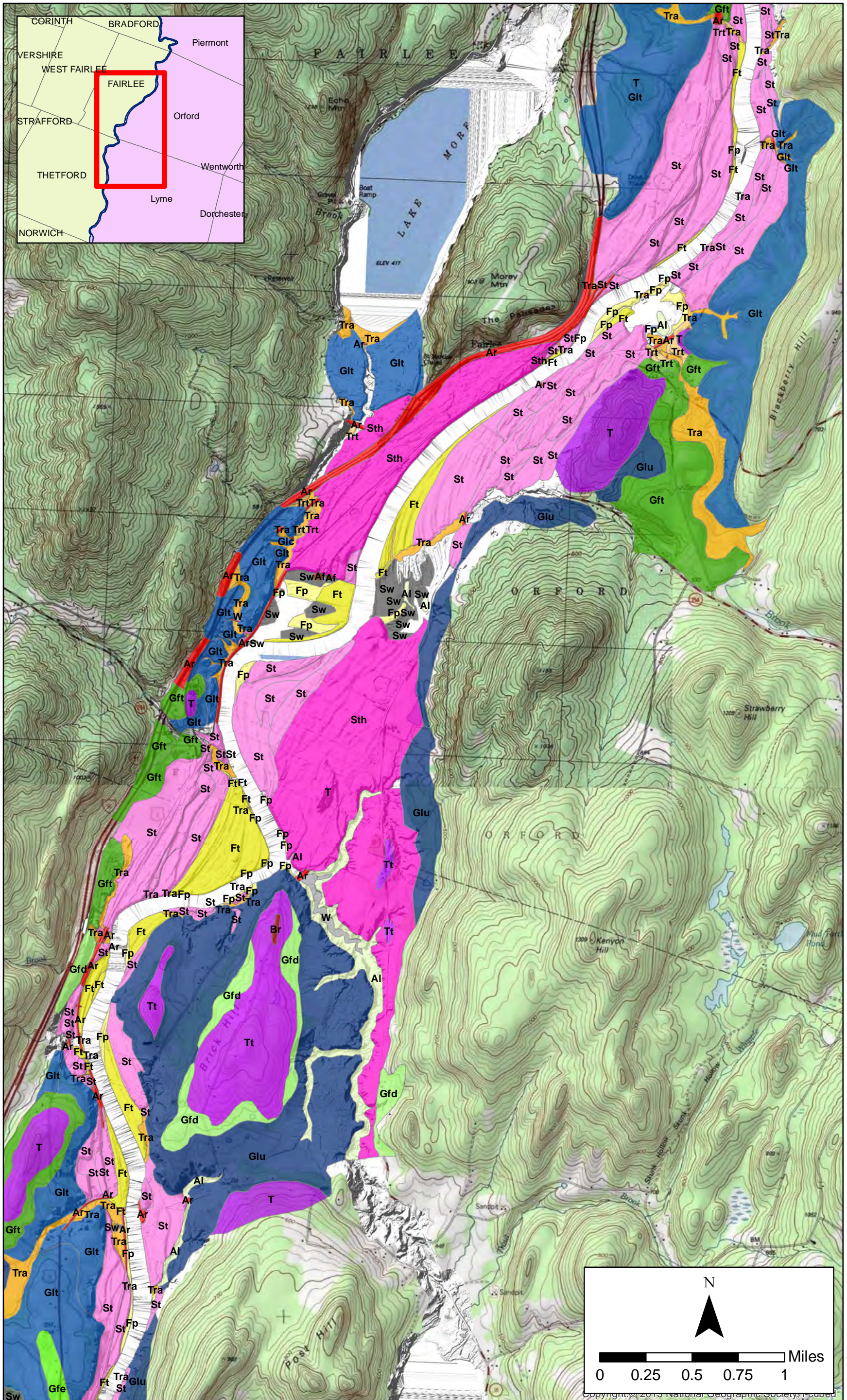
Appendix B. Surficial geologic maps. Plate 1 of 16.

Basemap imagery: USA Topo Maps and LiDAR hillshade.



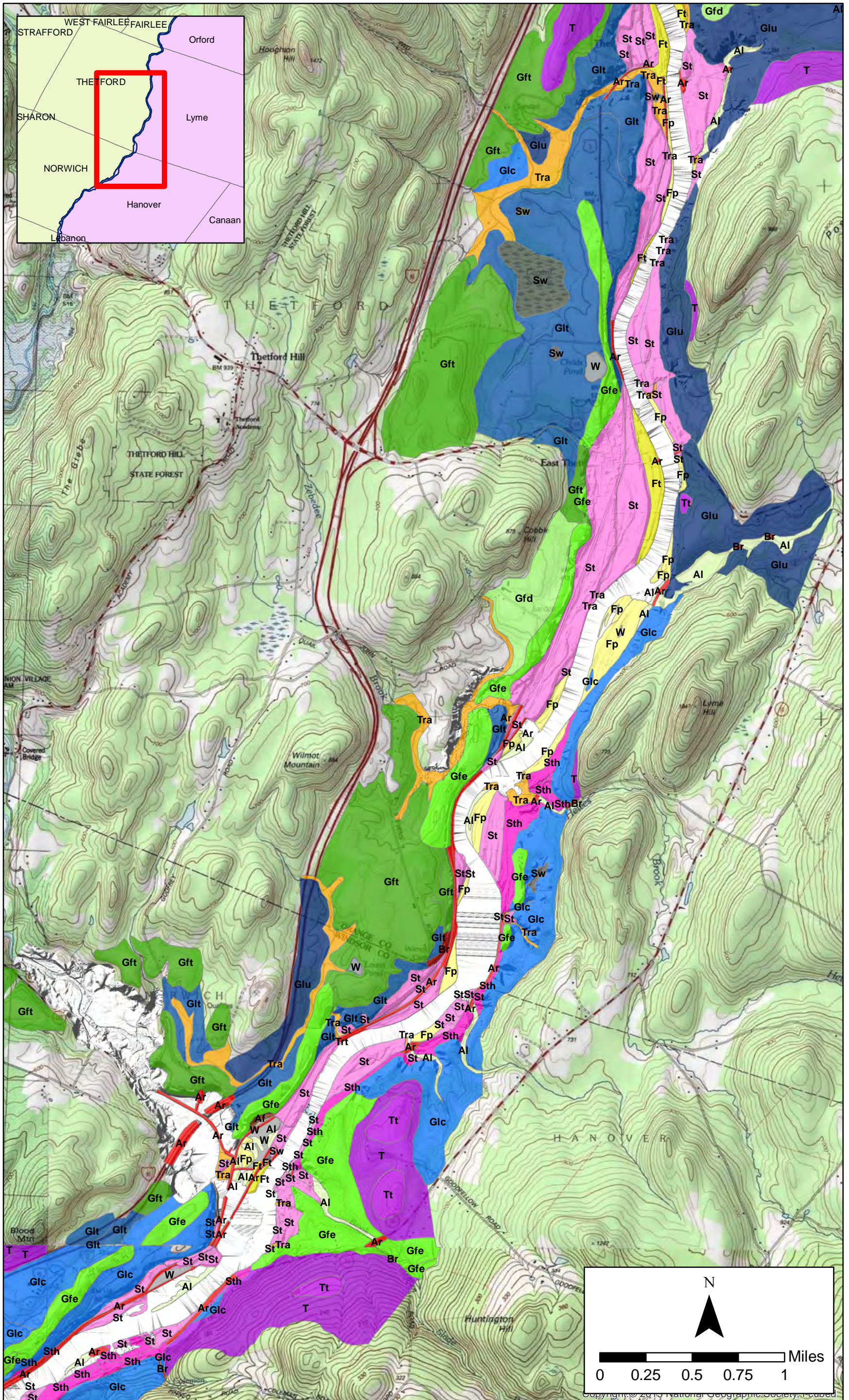
Appendix B. Surficial geologic maps. Plate 2 of 16.

Basemap imagery: USA Topo Maps and LiDAR hillshade.



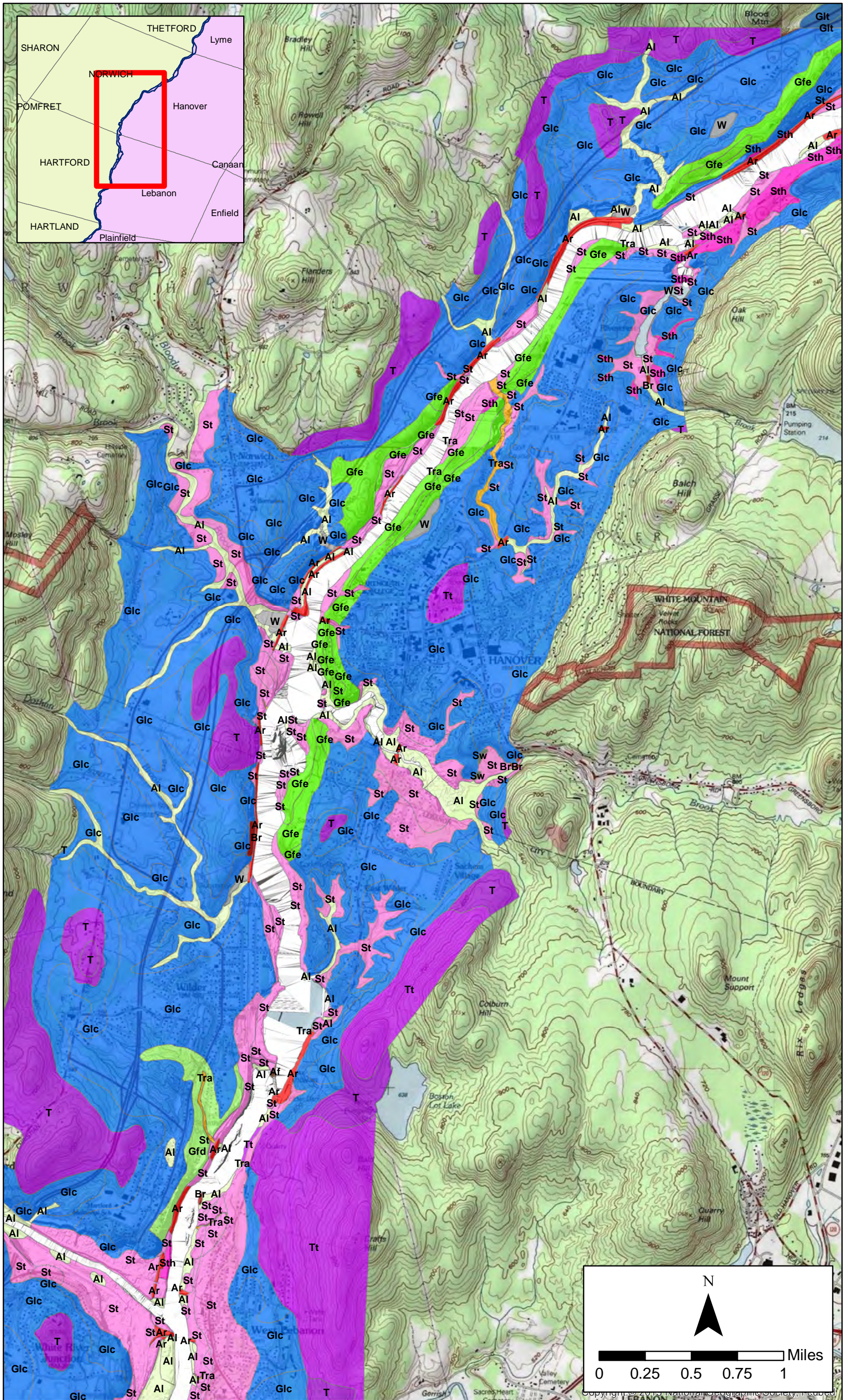
Appendix B. Surficial geologic maps. Plate 3 of 16.

Basemap imagery: USA Topo Maps and LiDAR hillshade.



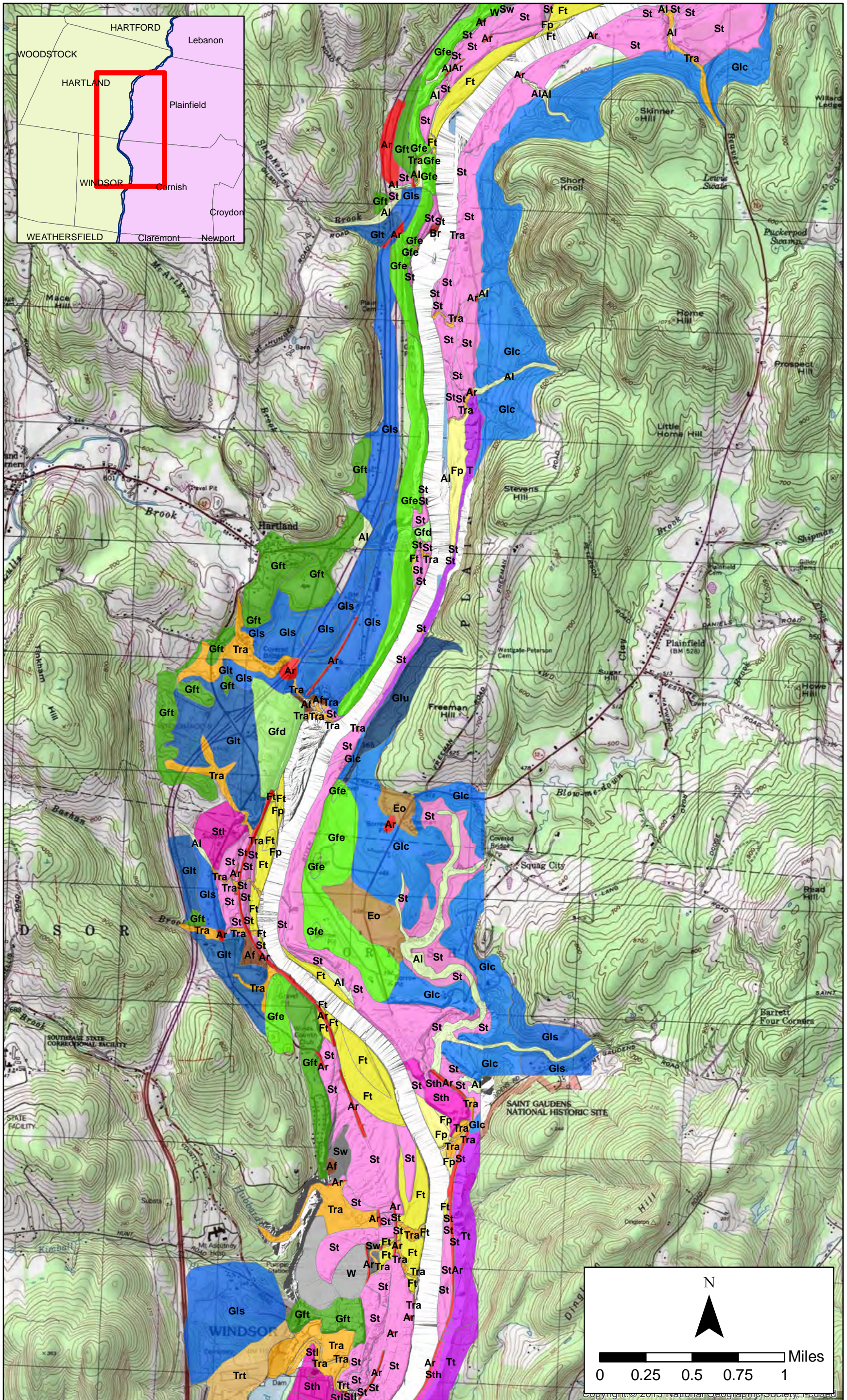
Appendix B. Surficial geologic maps. Plate 4 of 16.

Basemap imagery: USA Topo Maps and LiDAR hillshade.



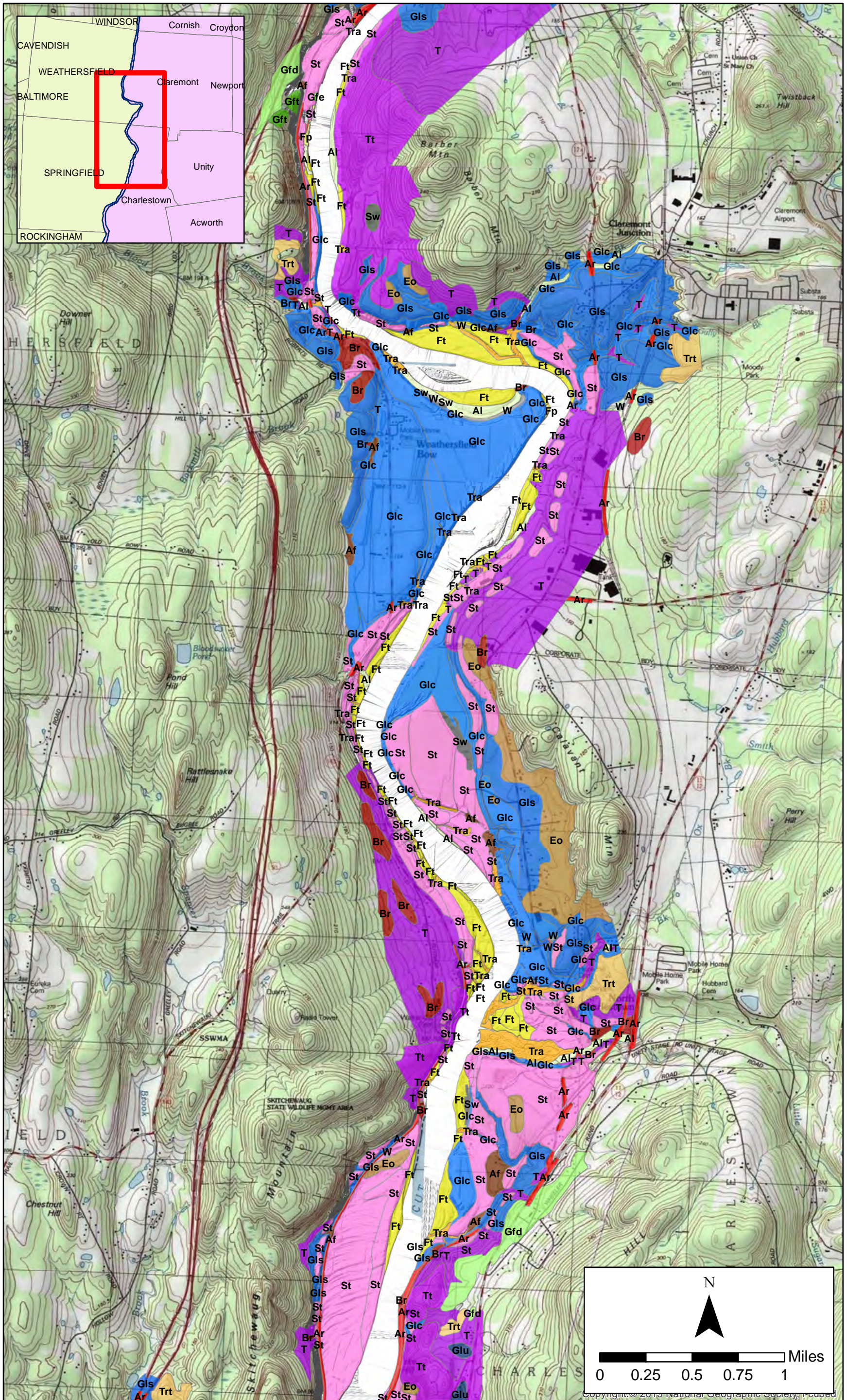
Appendix B. Surficial geologic maps. Plate 5 of 16.

Basemap imagery: USA Topo Maps and LiDAR hillshade.



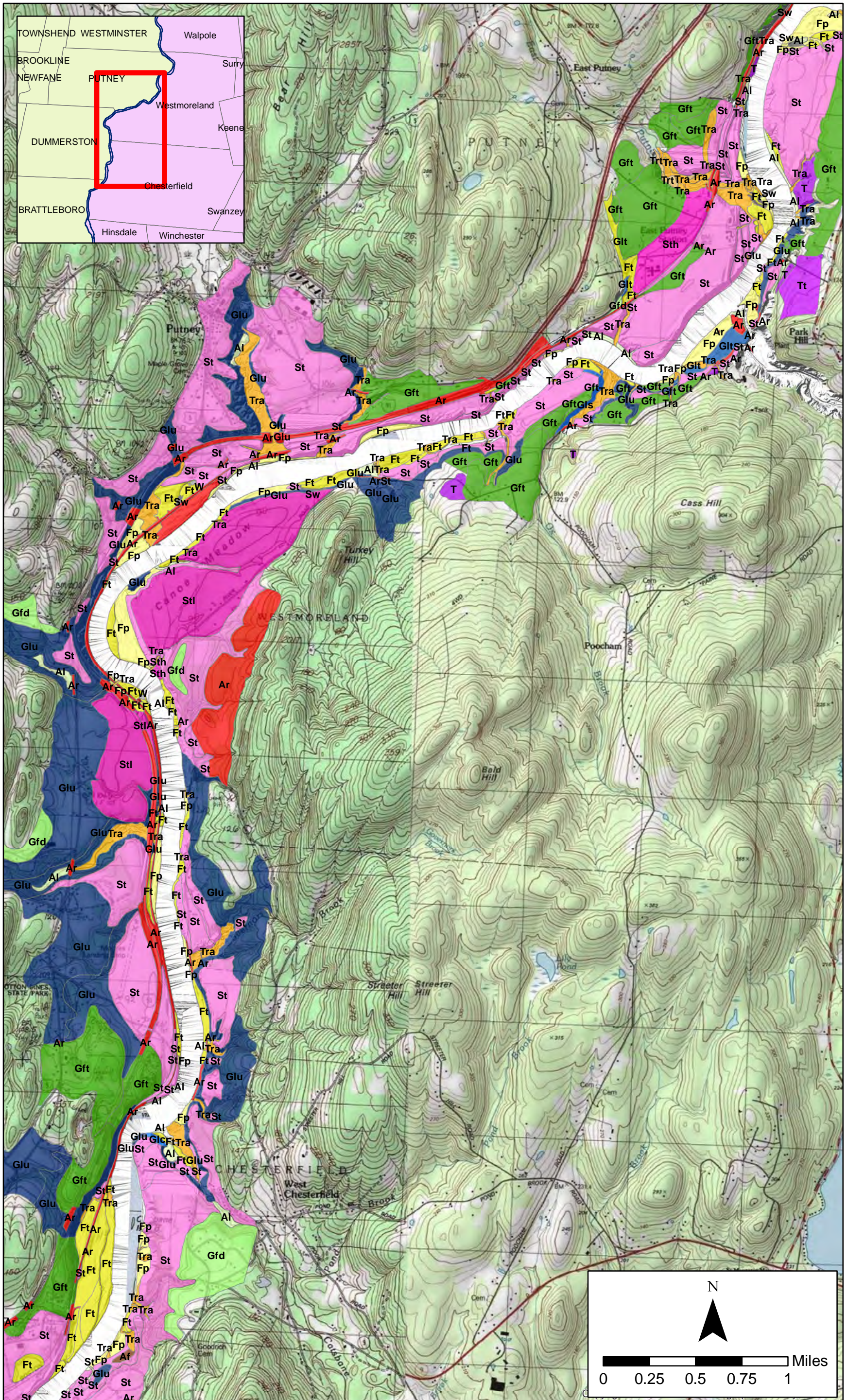
Appendix B. Surficial geologic maps. Plate 7 of 16.

Basemap imagery: USA Topo Maps and LiDAR hillshade.



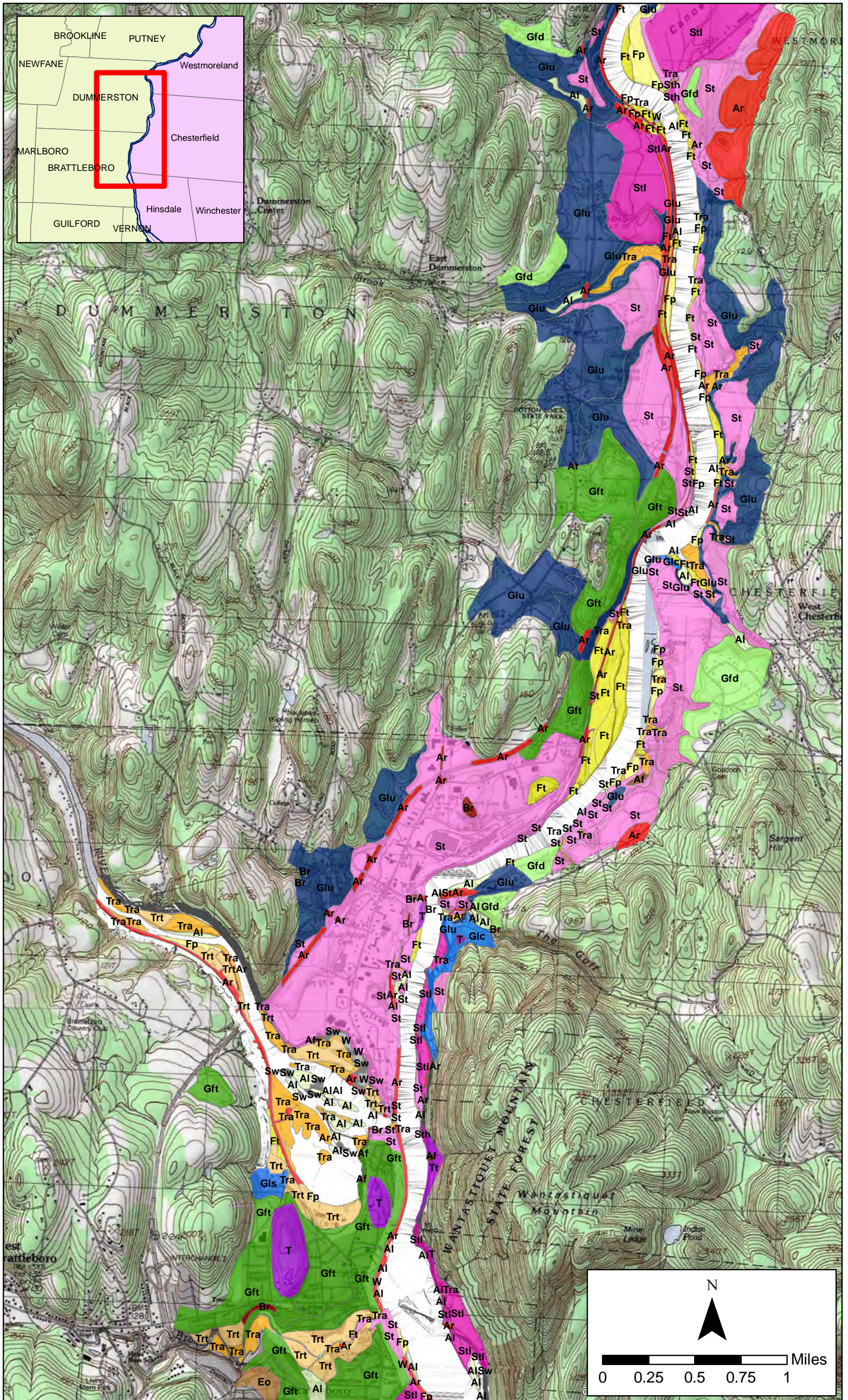
Appendix B. Surficial geologic maps. Plate 9 of 16.

Basemap imagery: USA Topo Maps and LiDAR hillshade.



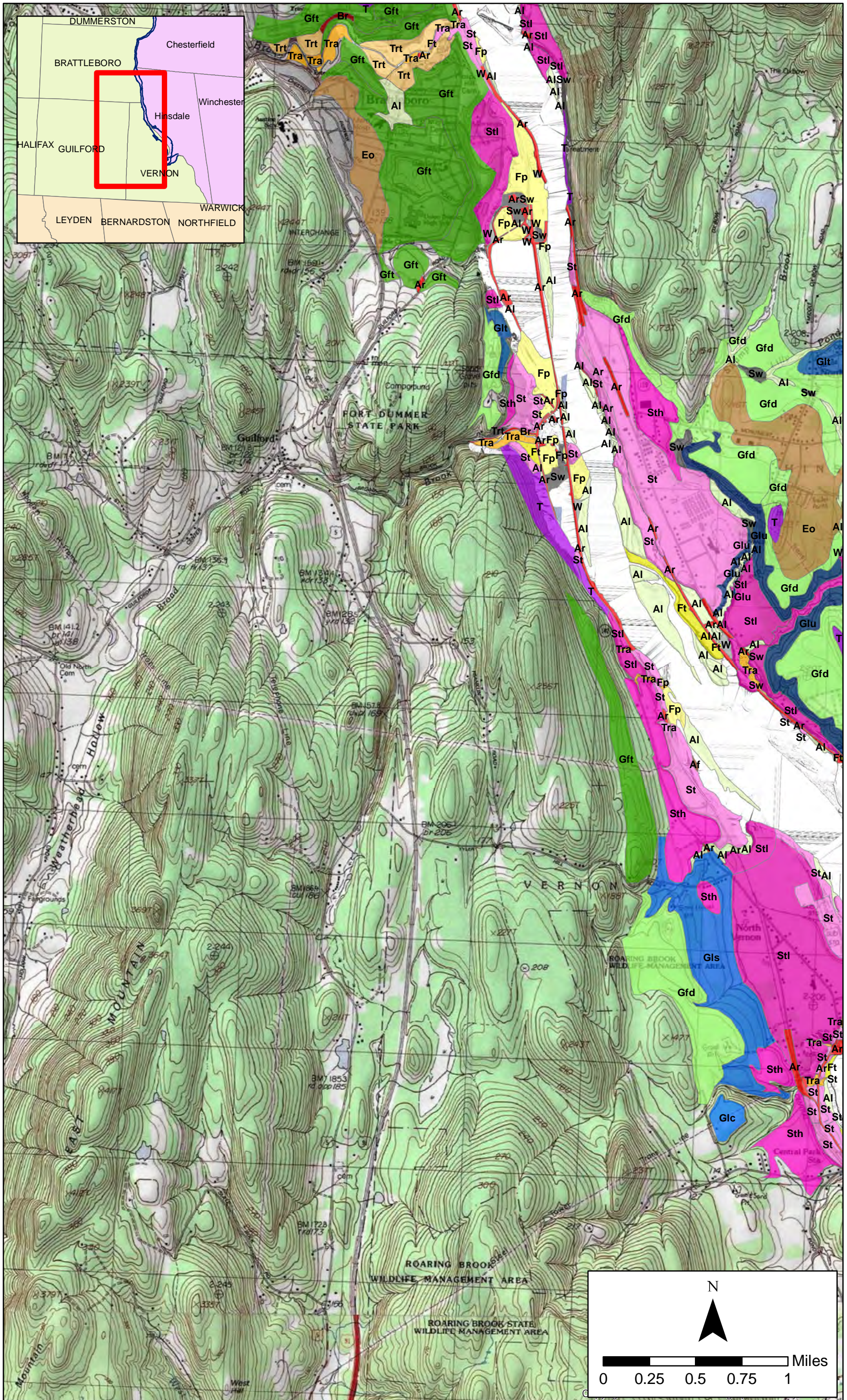
Appendix B. Surficial geologic maps. Plate 13 of 16.

Basemap imagery: USA Topo Maps and LiDAR hillshade.



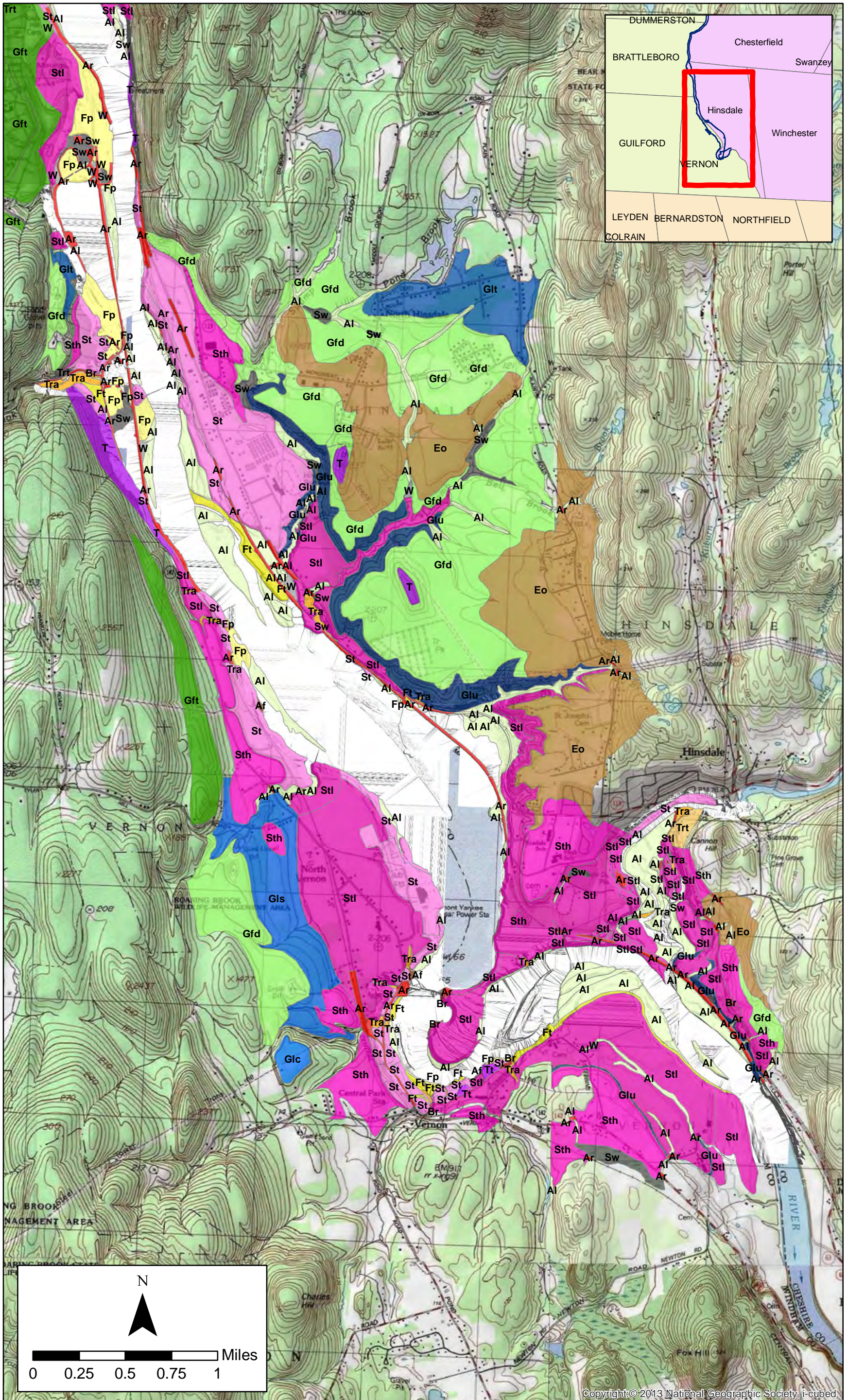
Appendix B. Surficial geologic maps. Plate 14 of 16.

Basemap imagery: USA Topo Maps and LiDAR hillshade.



Appendix B. Surficial geologic maps. Plate 15 of 16.

Basemap imagery: USA Topo Maps and LiDAR hillshade.



Appendix B. Surficial geologic maps. Plate 16 of 16.

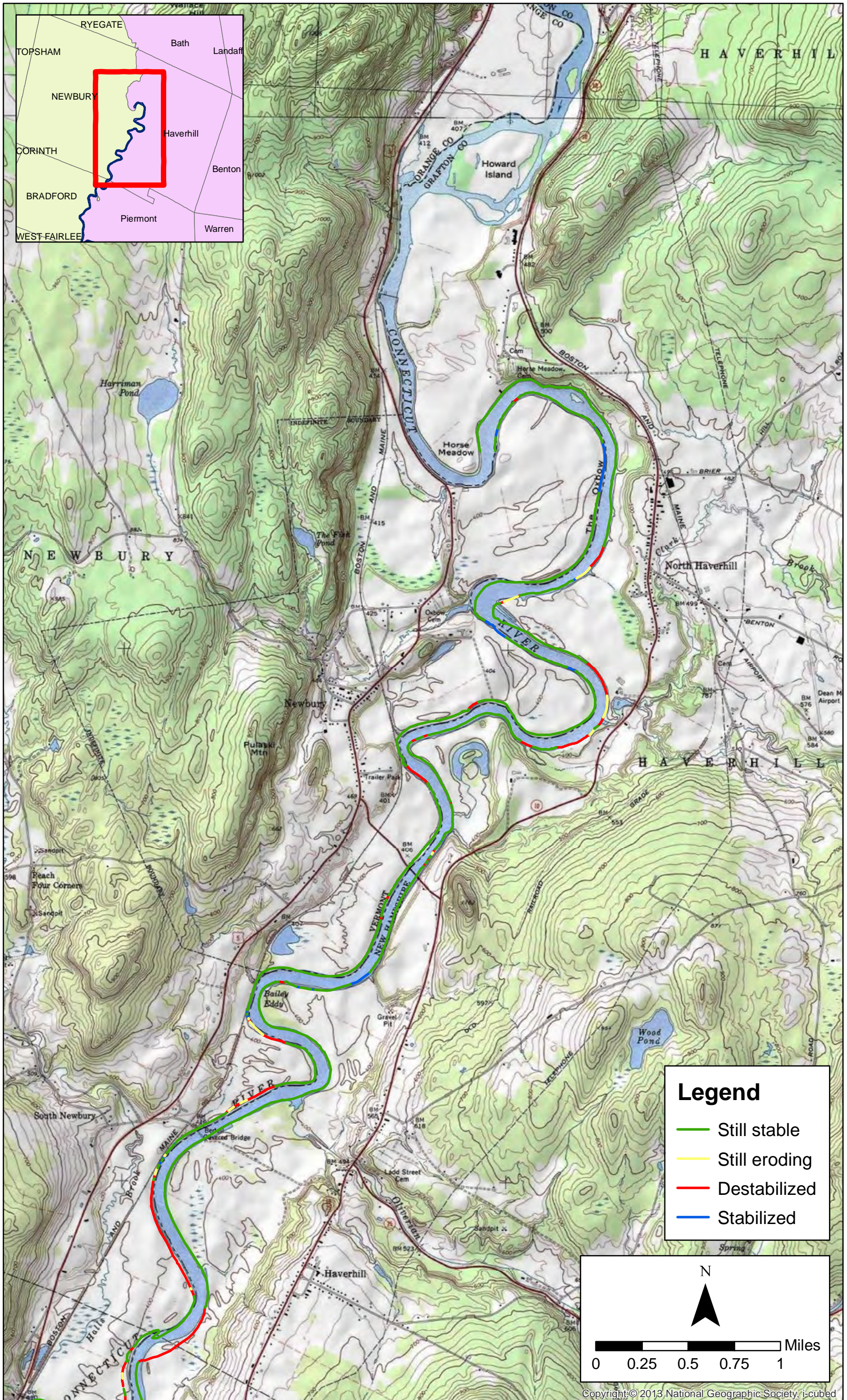
Basemap imagery: USA Topo Maps and LiDAR hillshade.

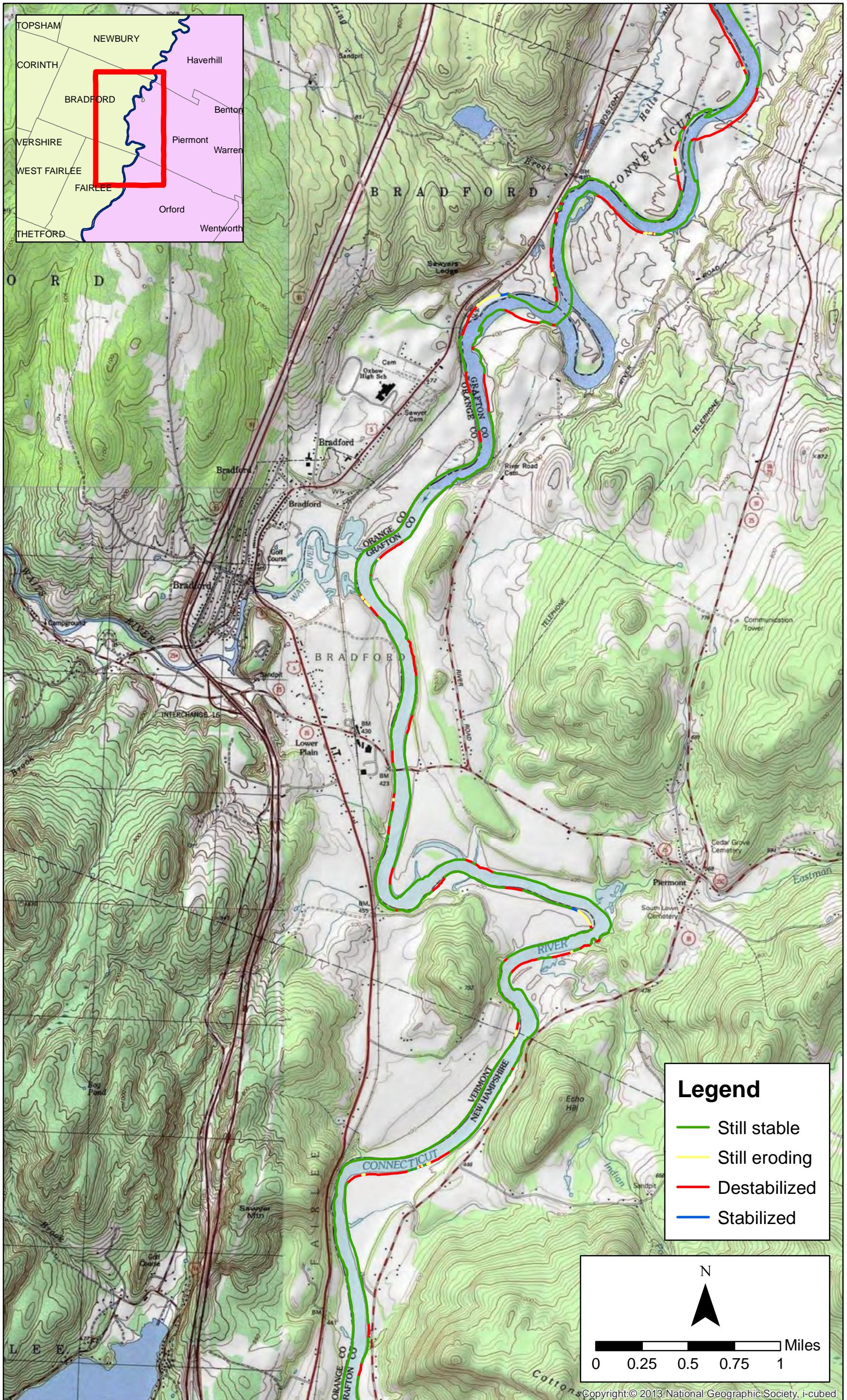
[This page intentionally left blank.]

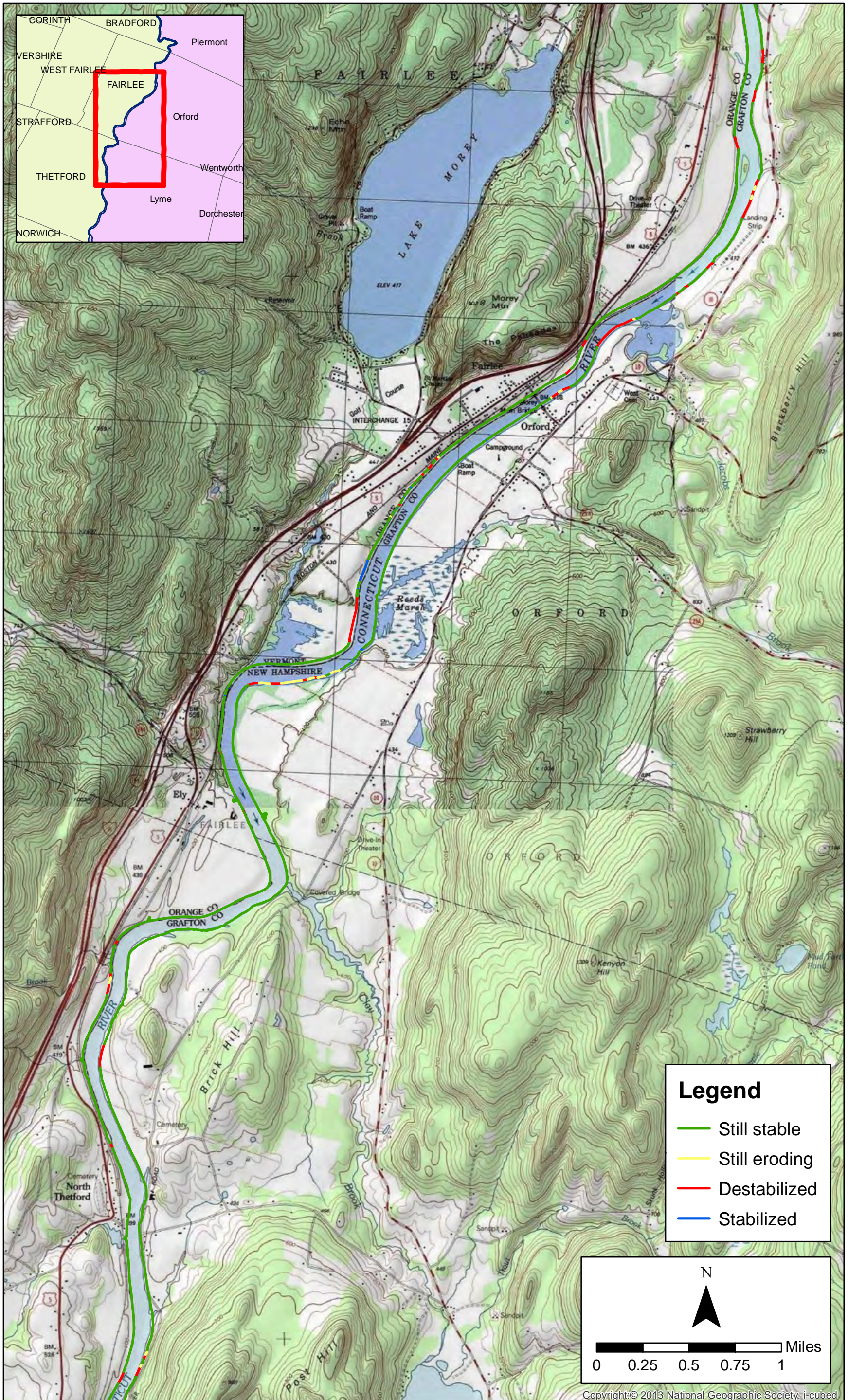
APPENDIX D

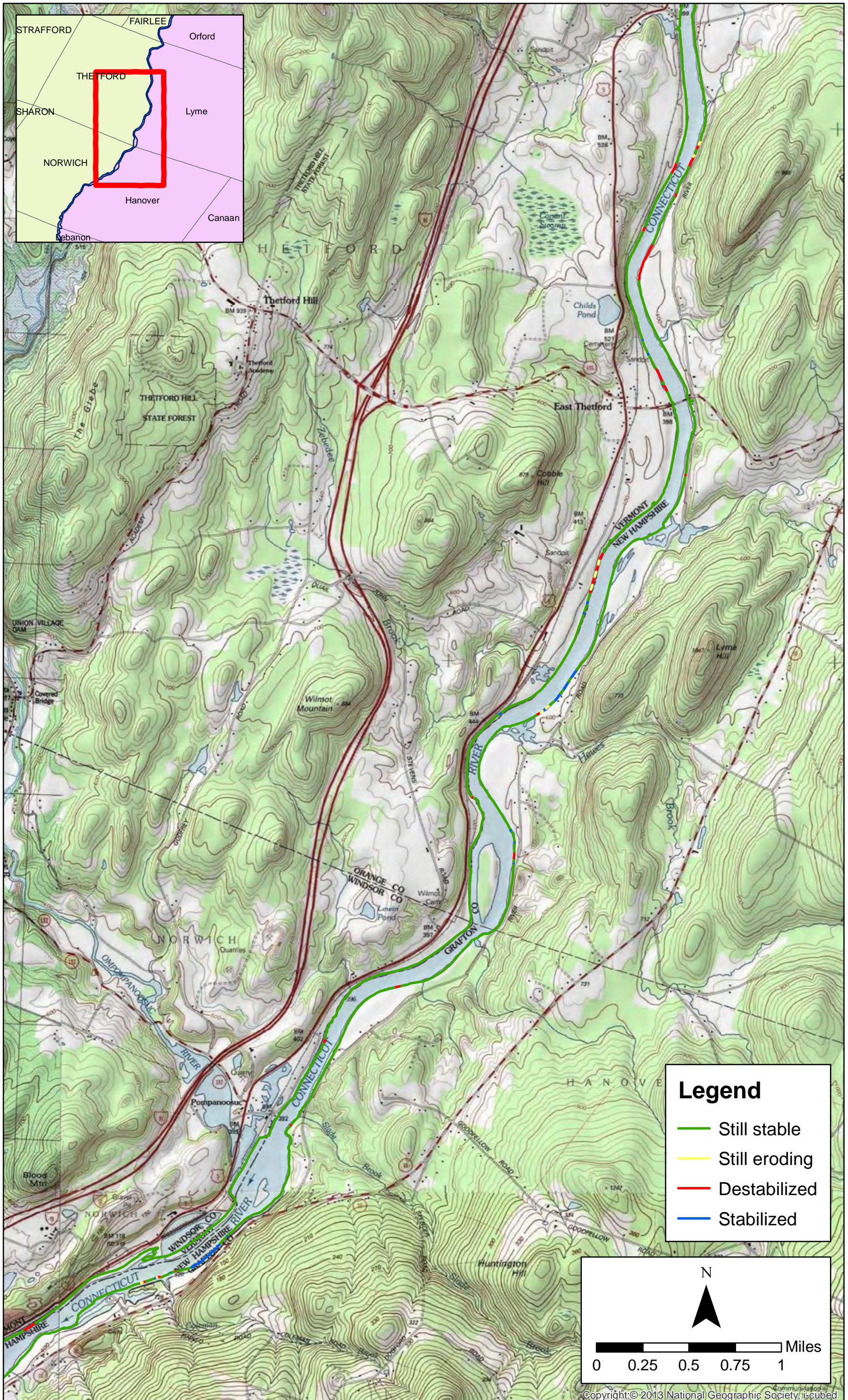
Comparison of erosion maps from 1955, 1979, and 2014

[This page intentionally left blank.]



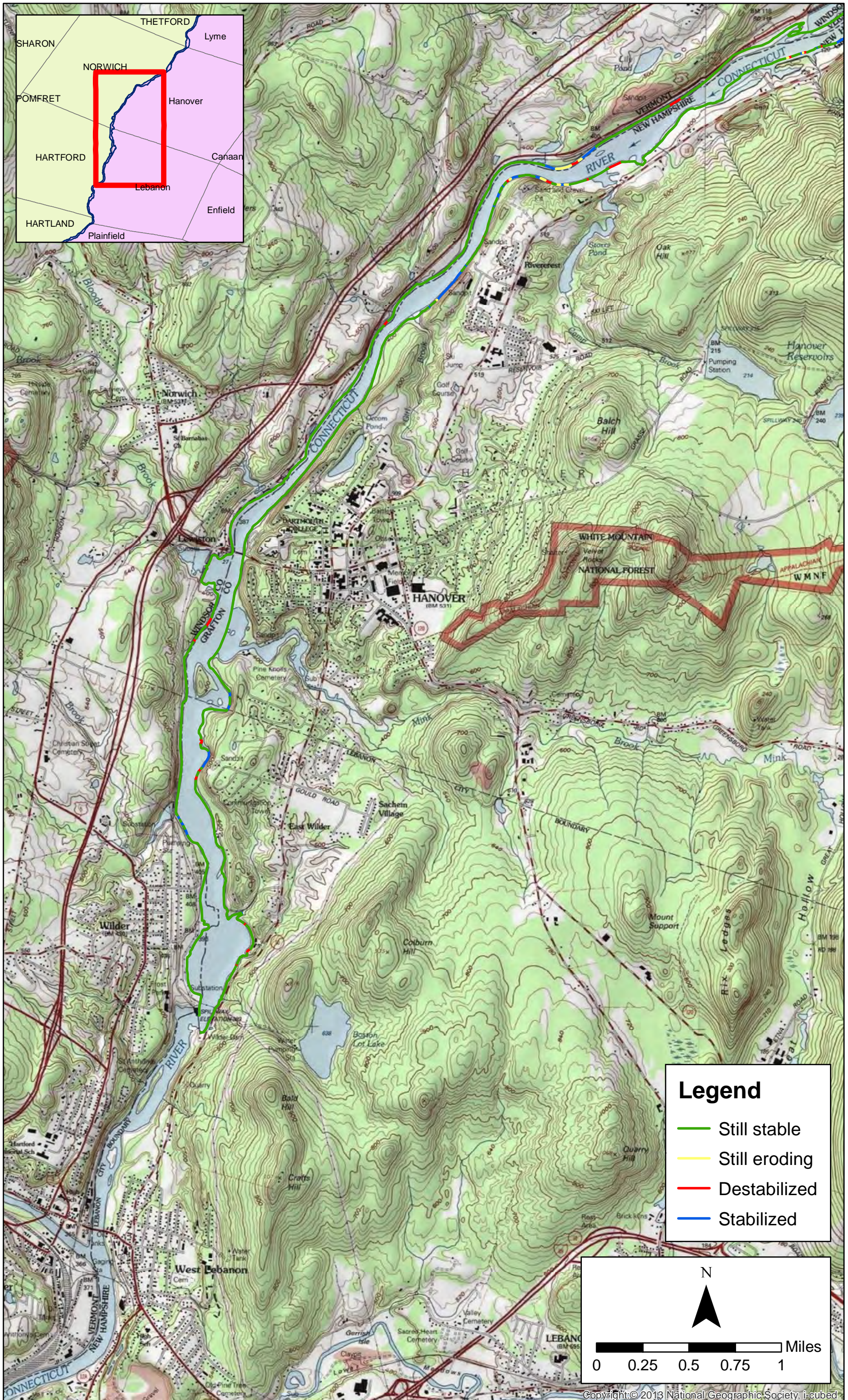


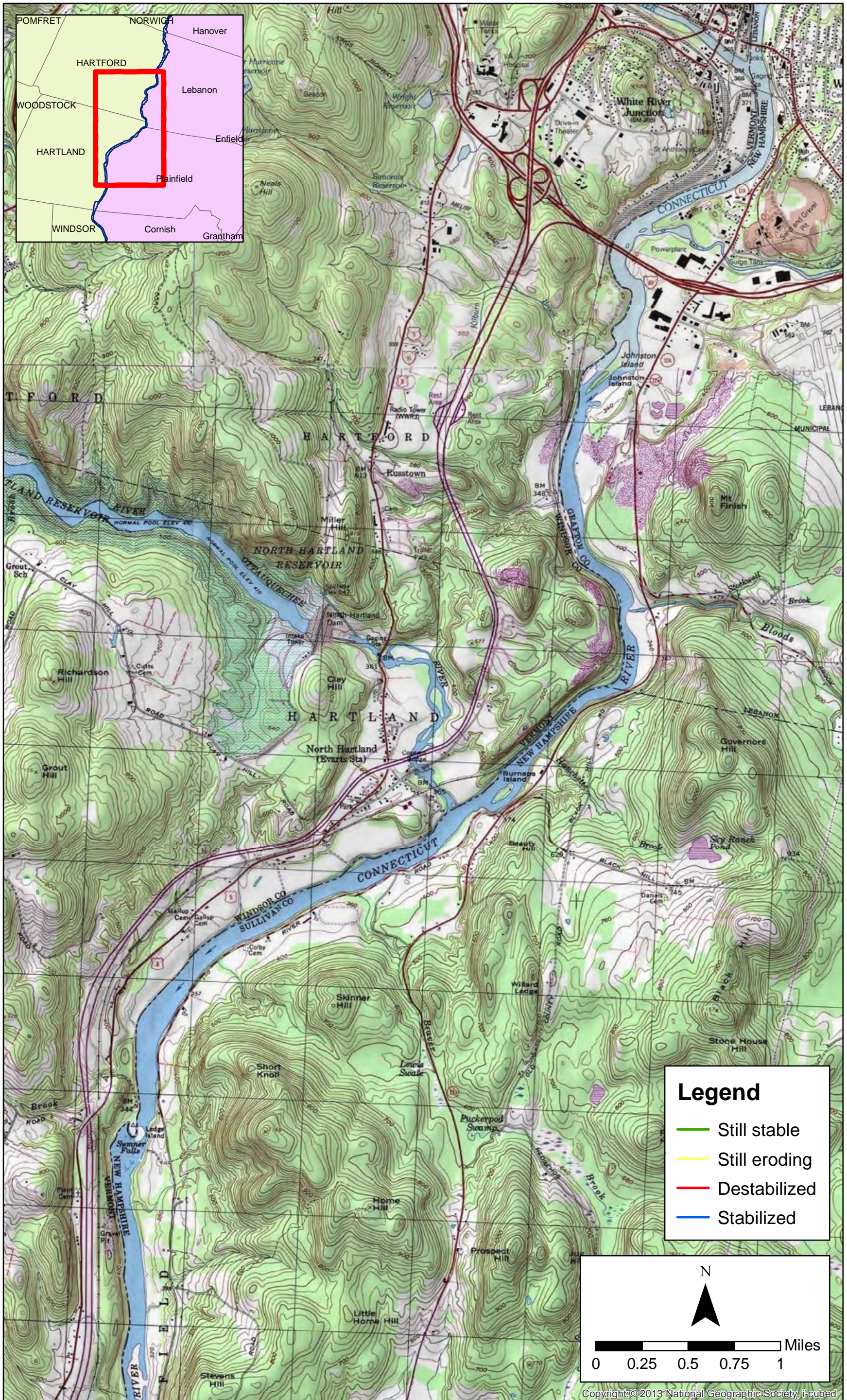


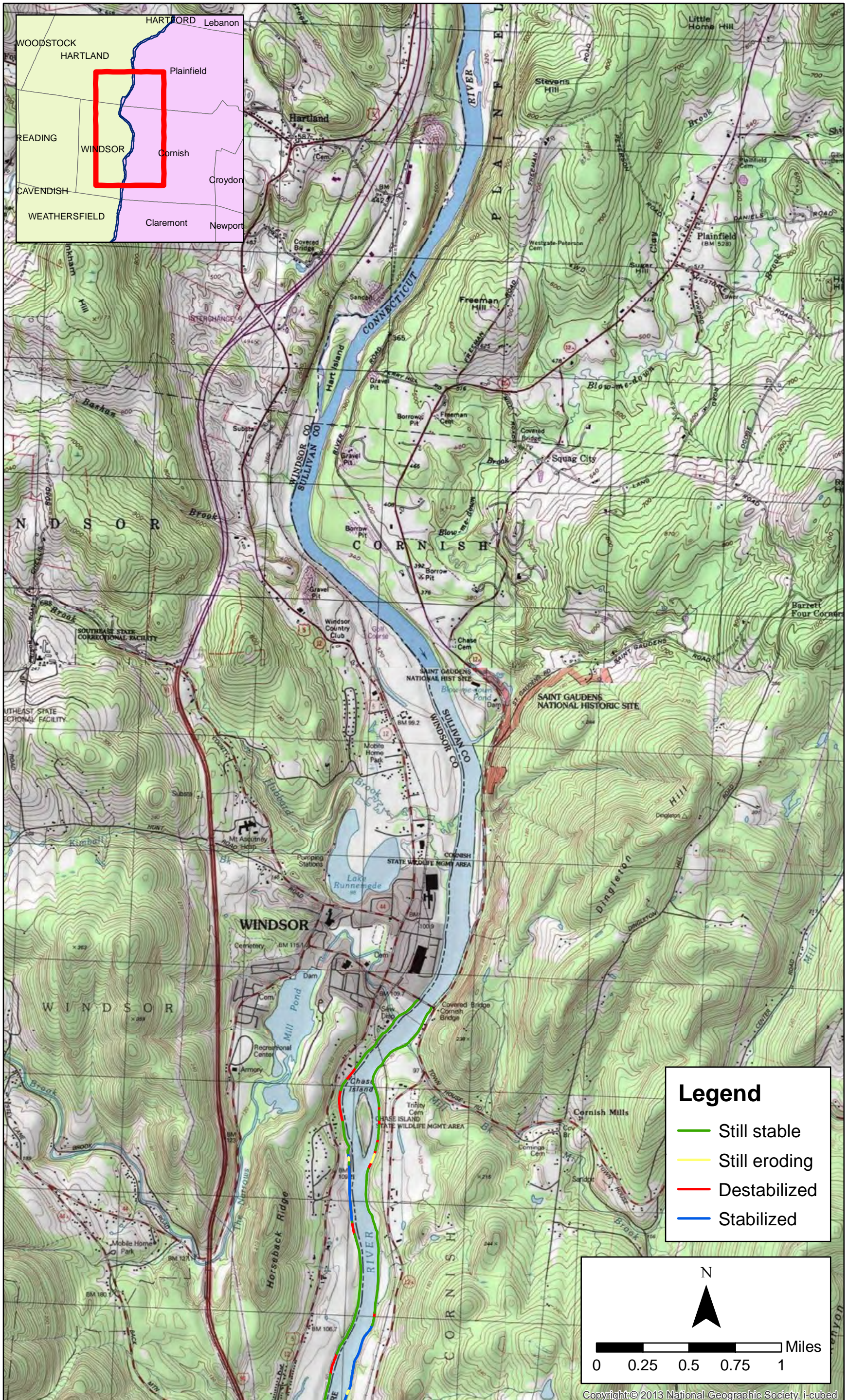


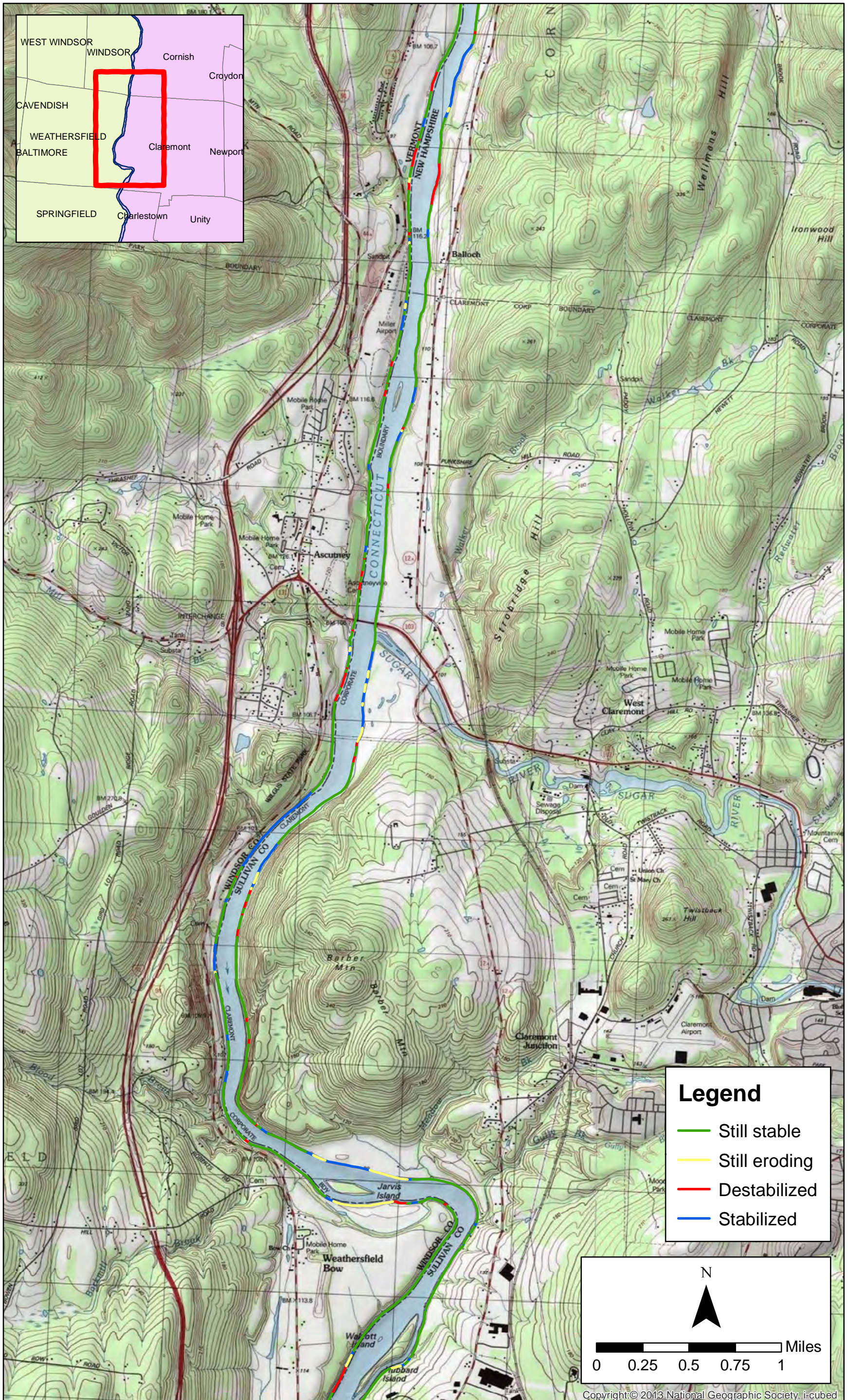
Appendix D. Comparison of 1958 and 2014 erosion. Plate 4 of 14.

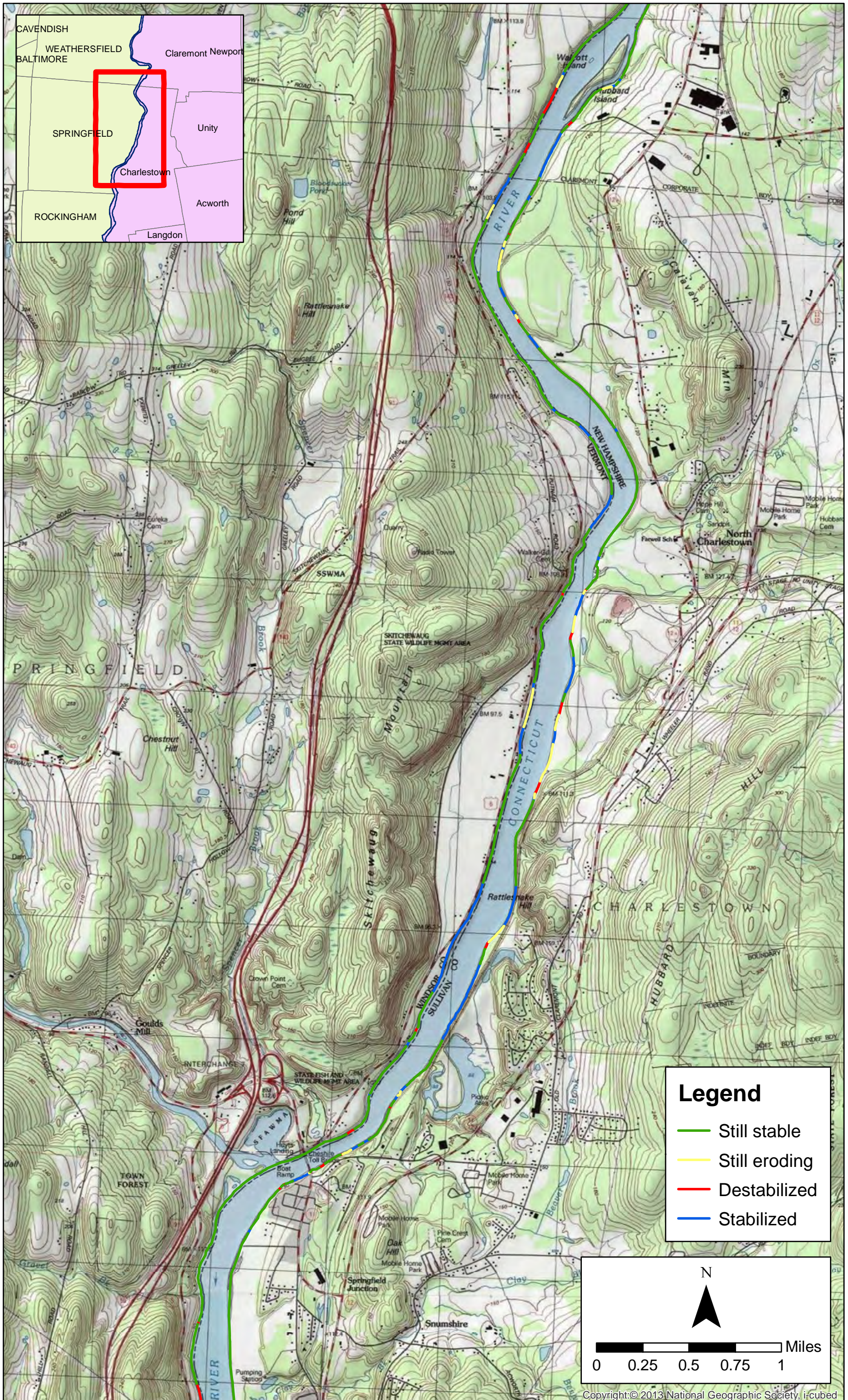
Basemap imagery: USA Topo Maps.

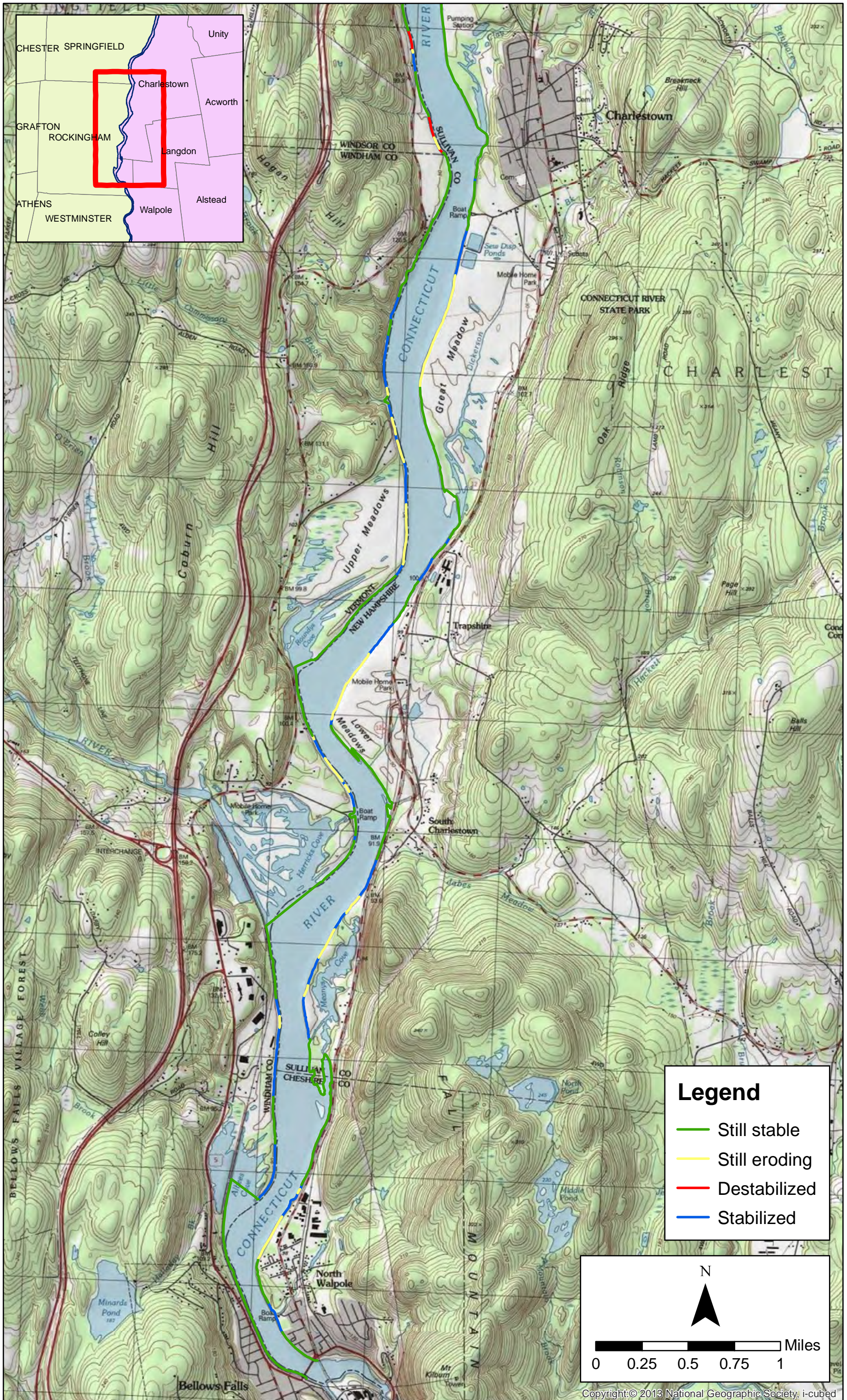


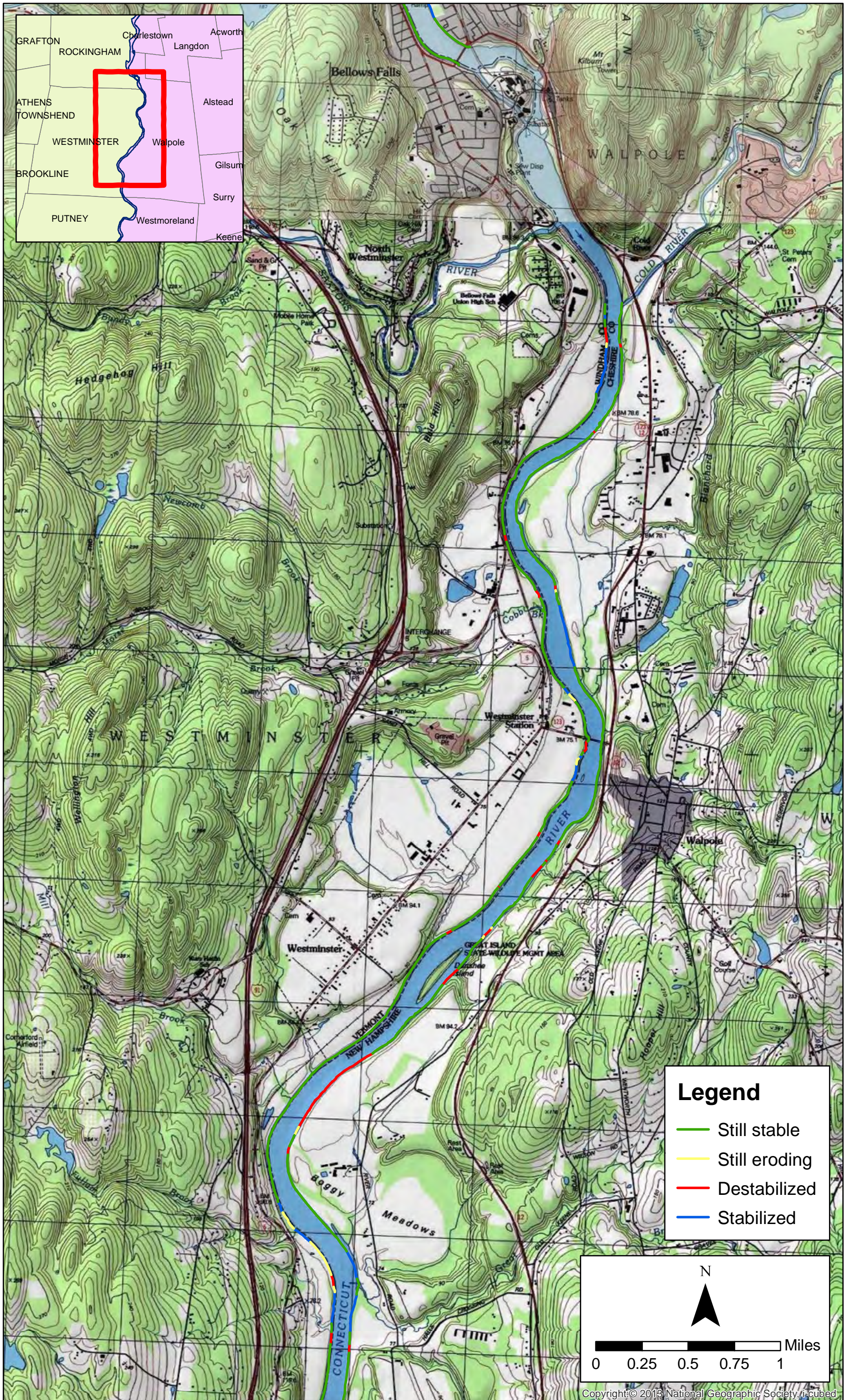


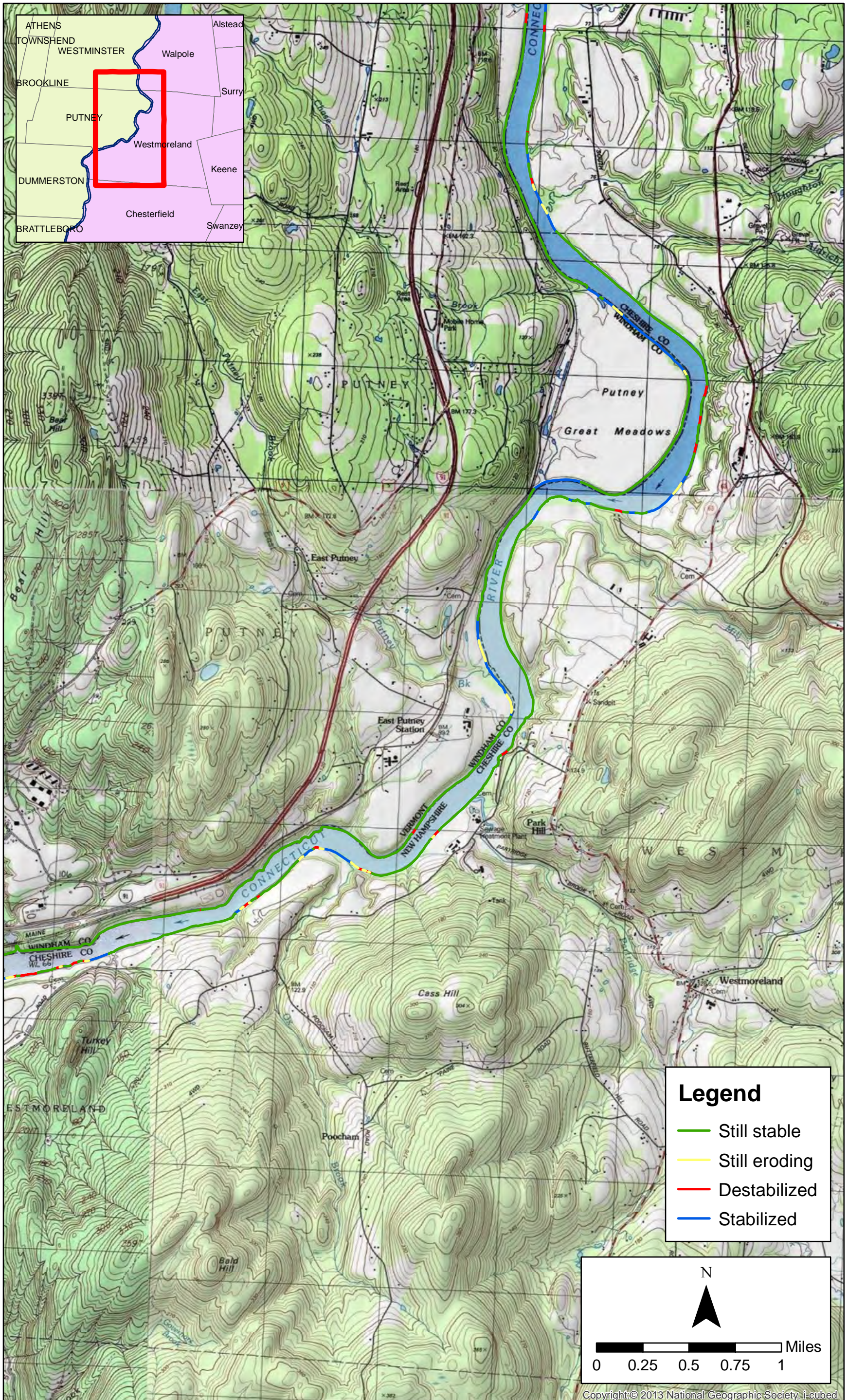


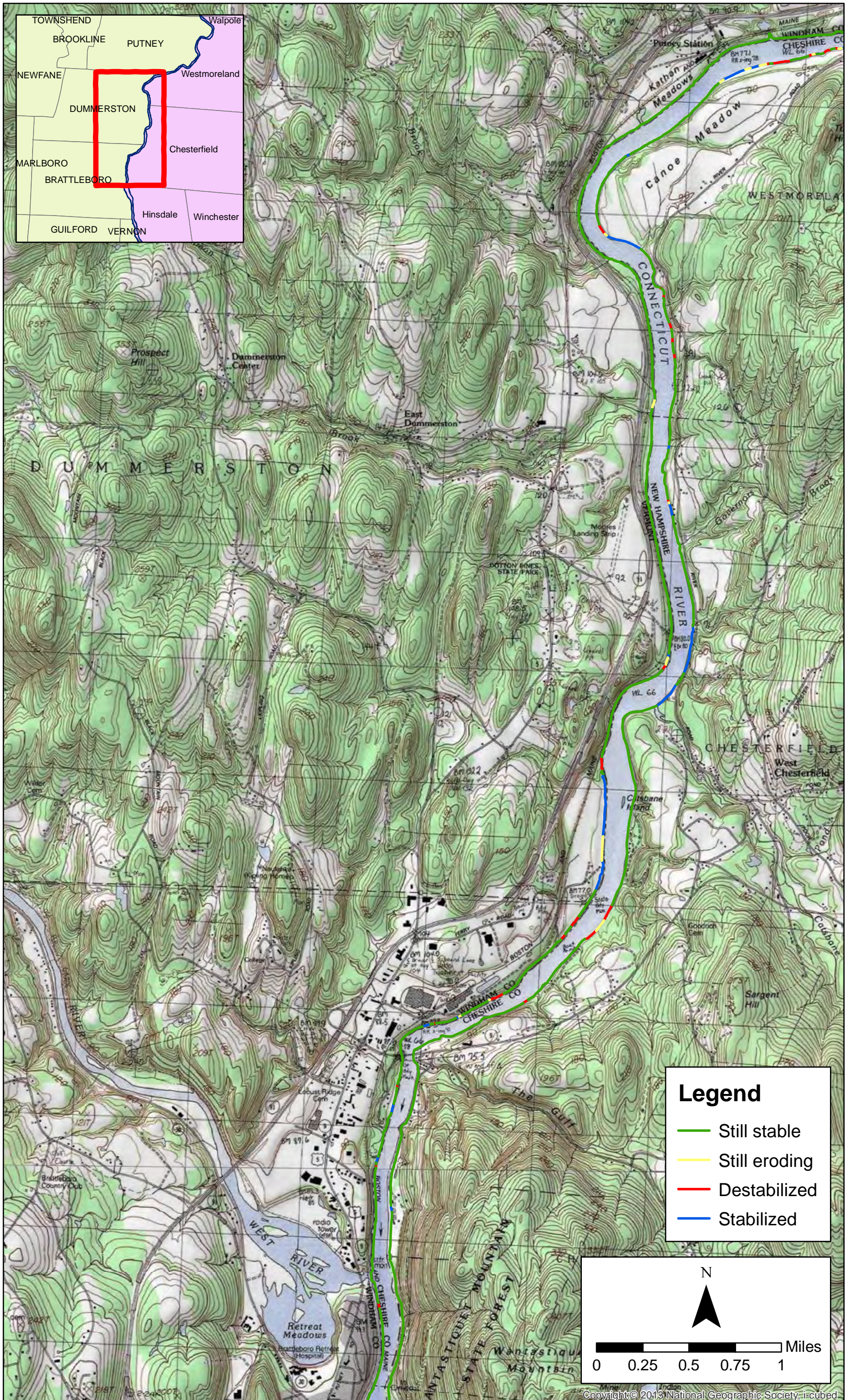


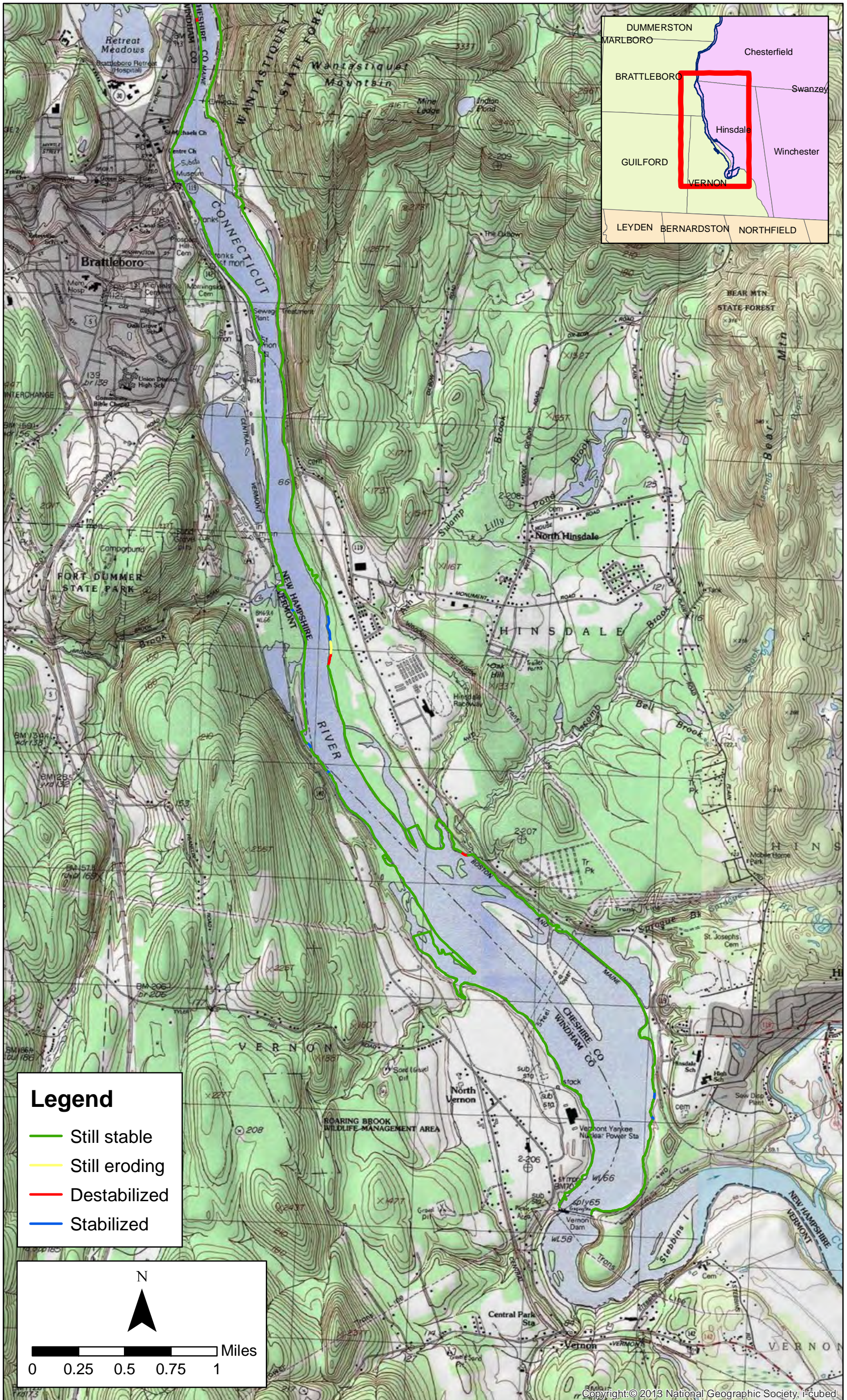






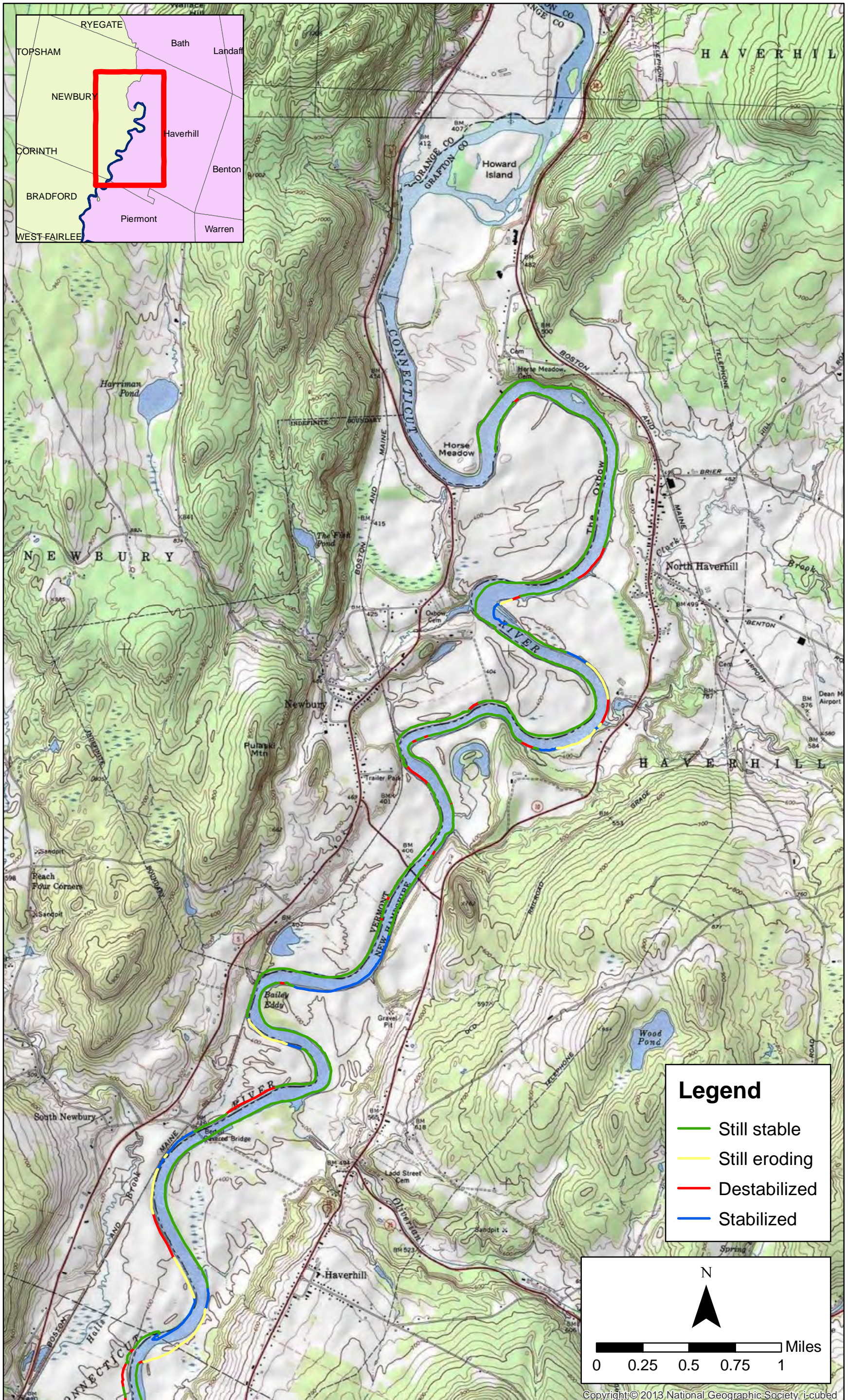


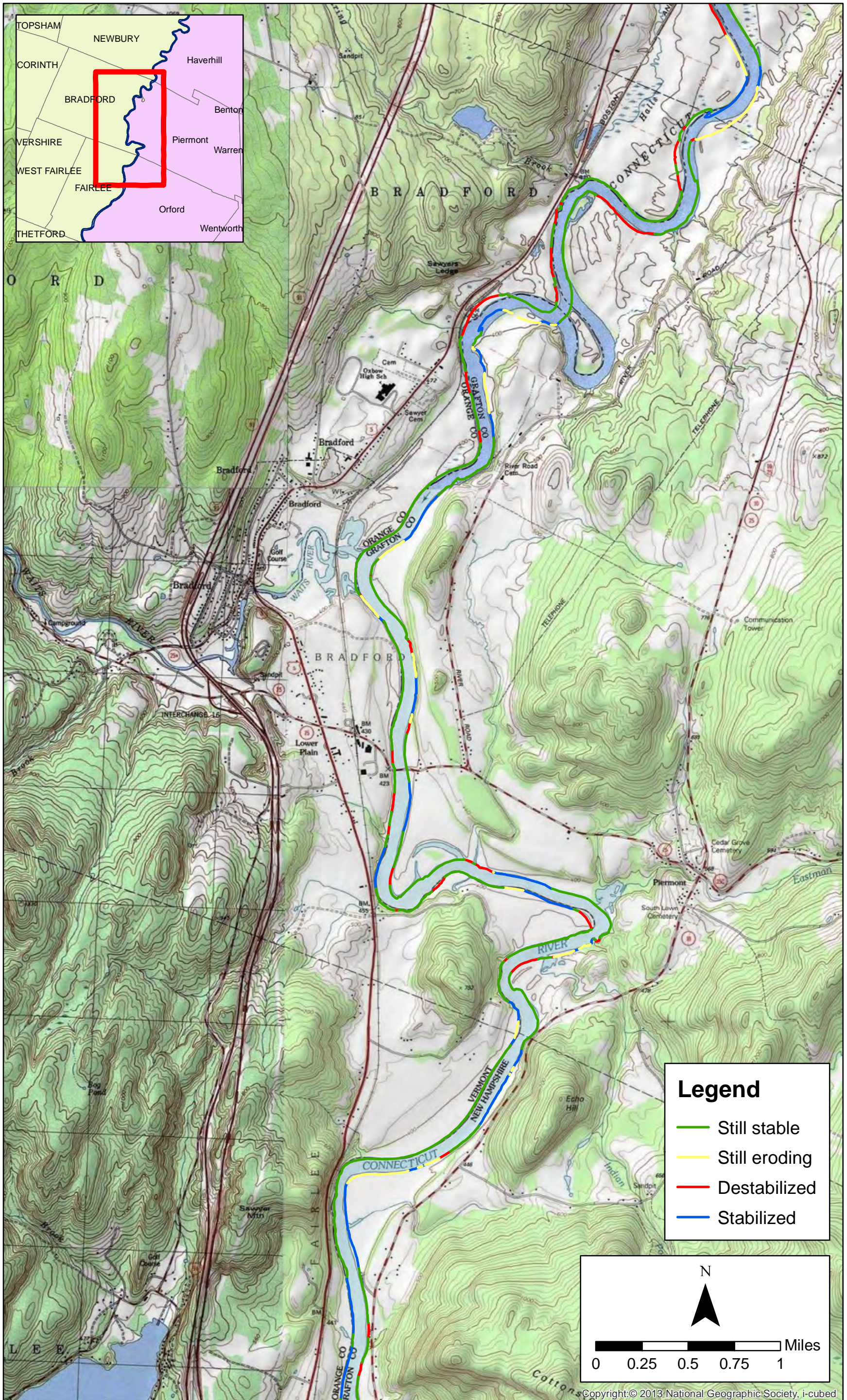




Appendix D. Comparison of 1958 and 2014 erosion. Plate 14 of 14.

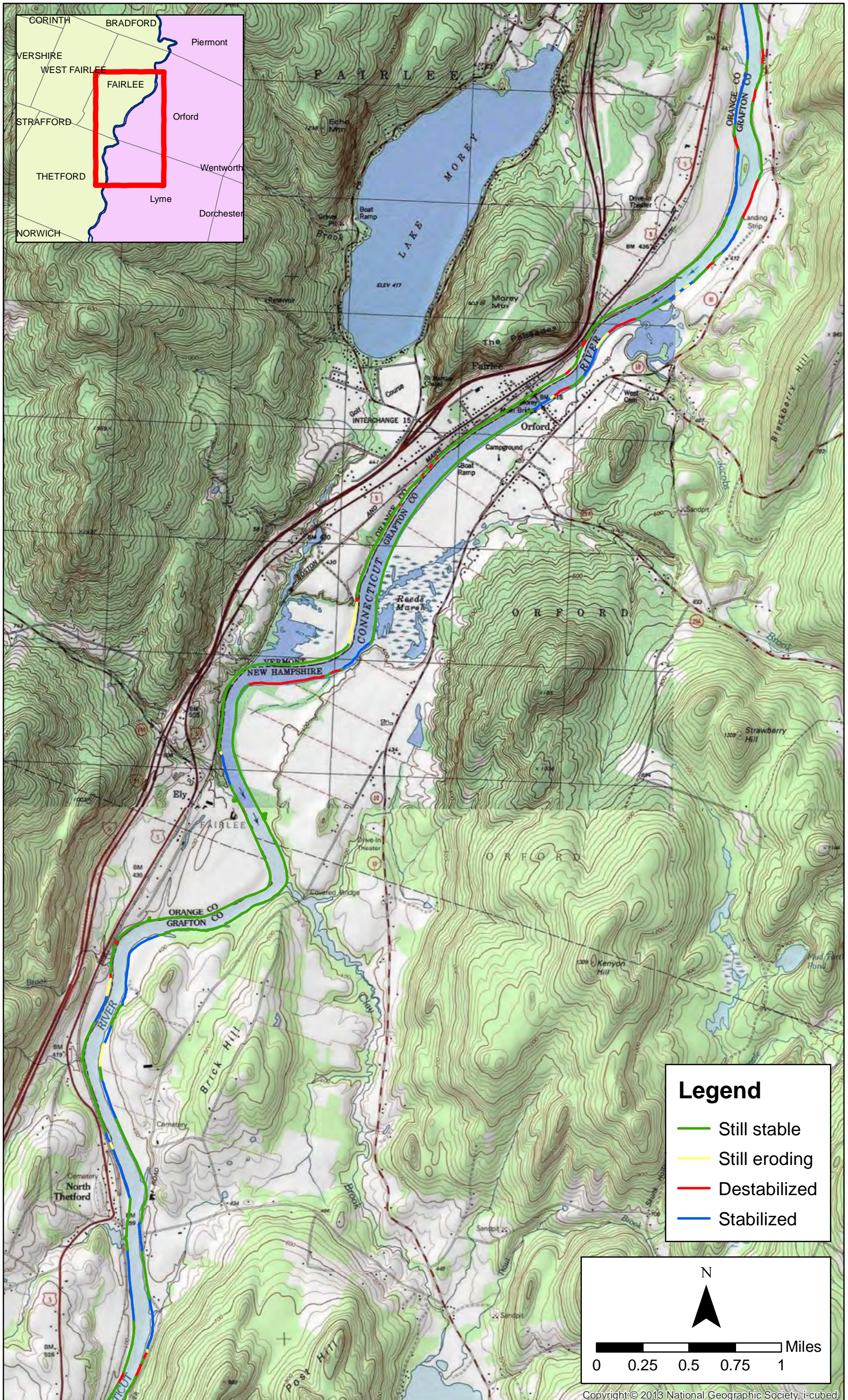
Basemap imagery: USA Topo Maps.





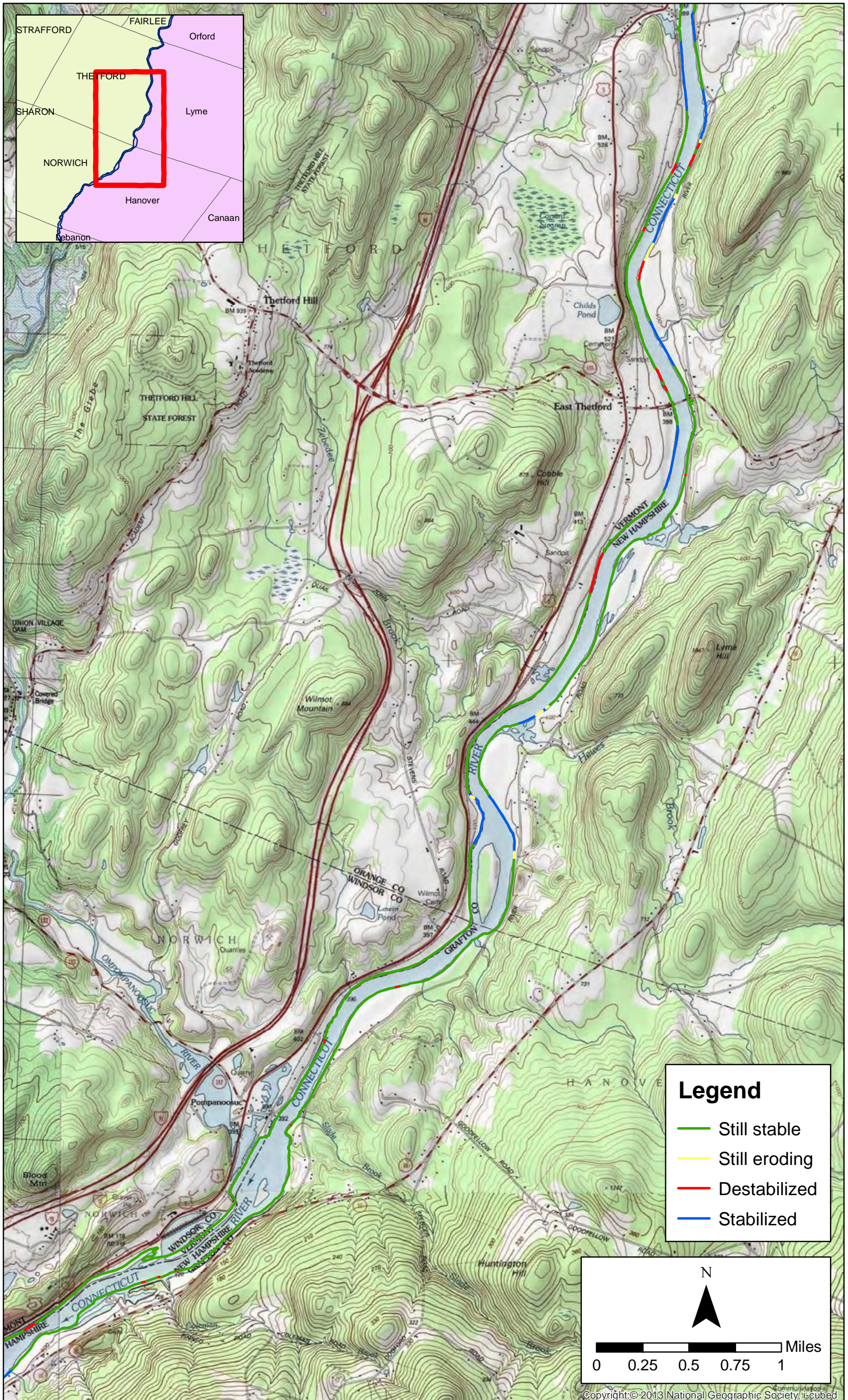
Appendix D. Comparison of 1978 and 2014 erosion. Plate 2 of 14.

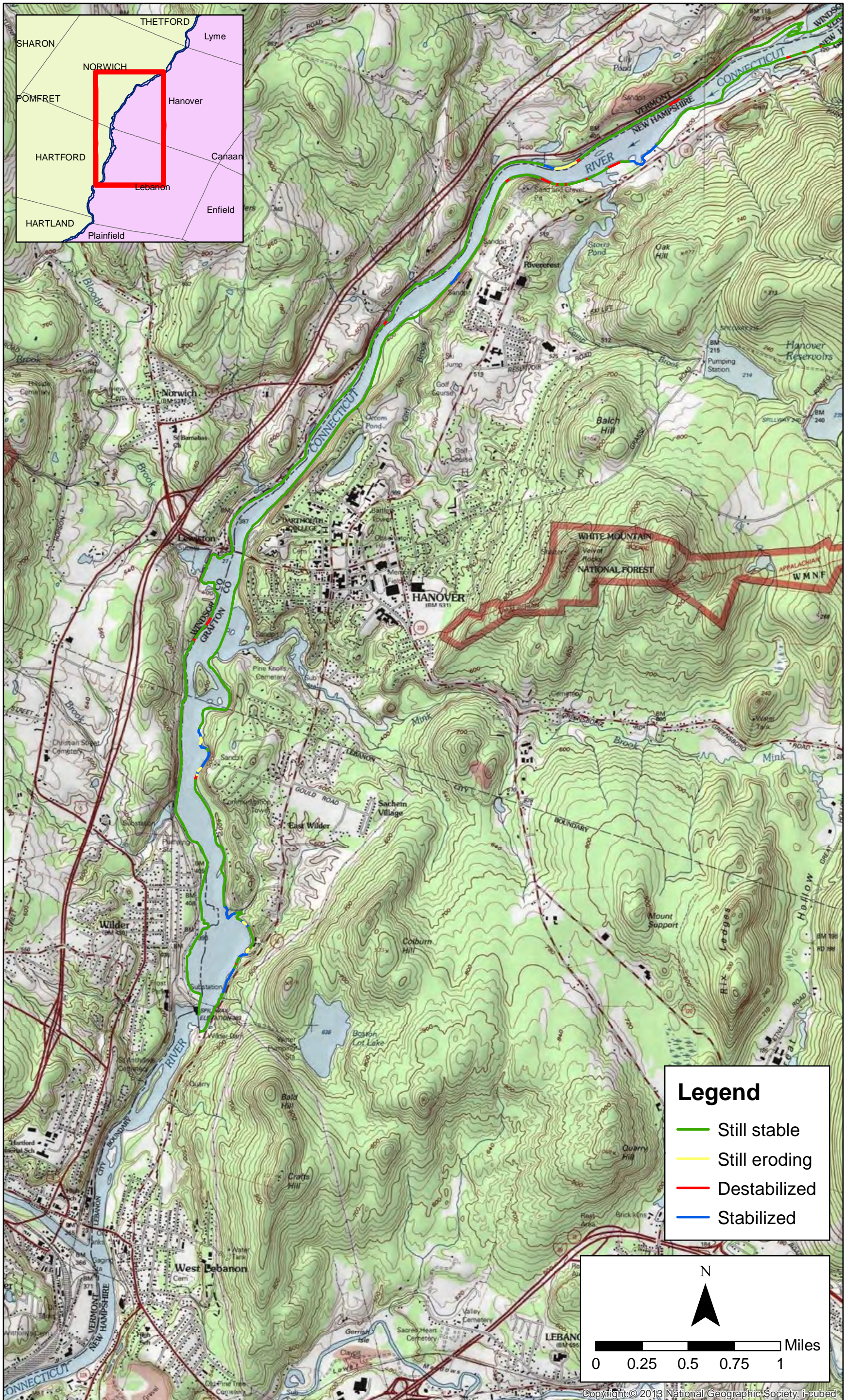
Basemap imagery: USA Topo Maps.

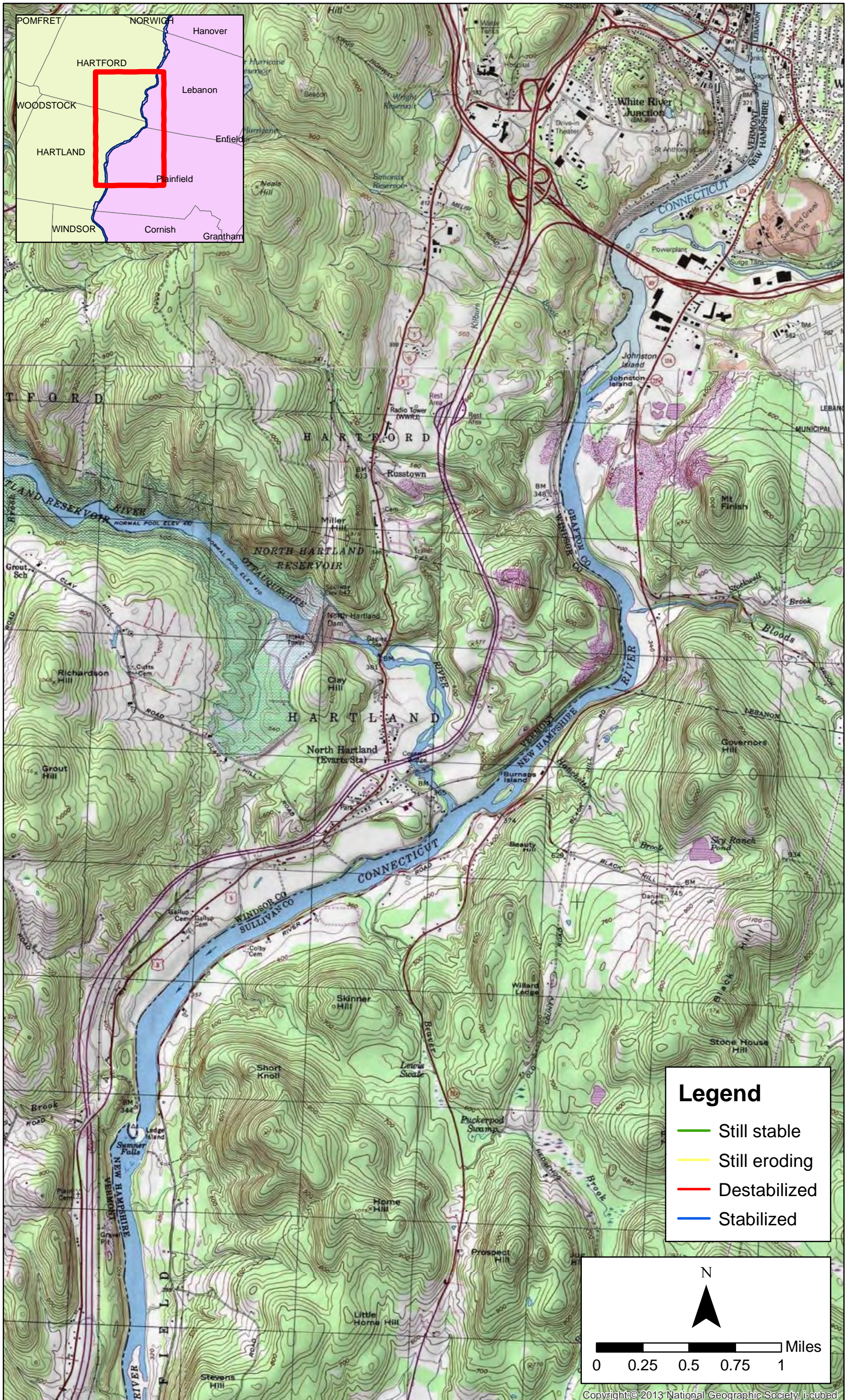


Appendix D. Comparison of 1978 and 2014 erosion. Plate 3 of 14.

Basemap imagery: USA Topo Maps.

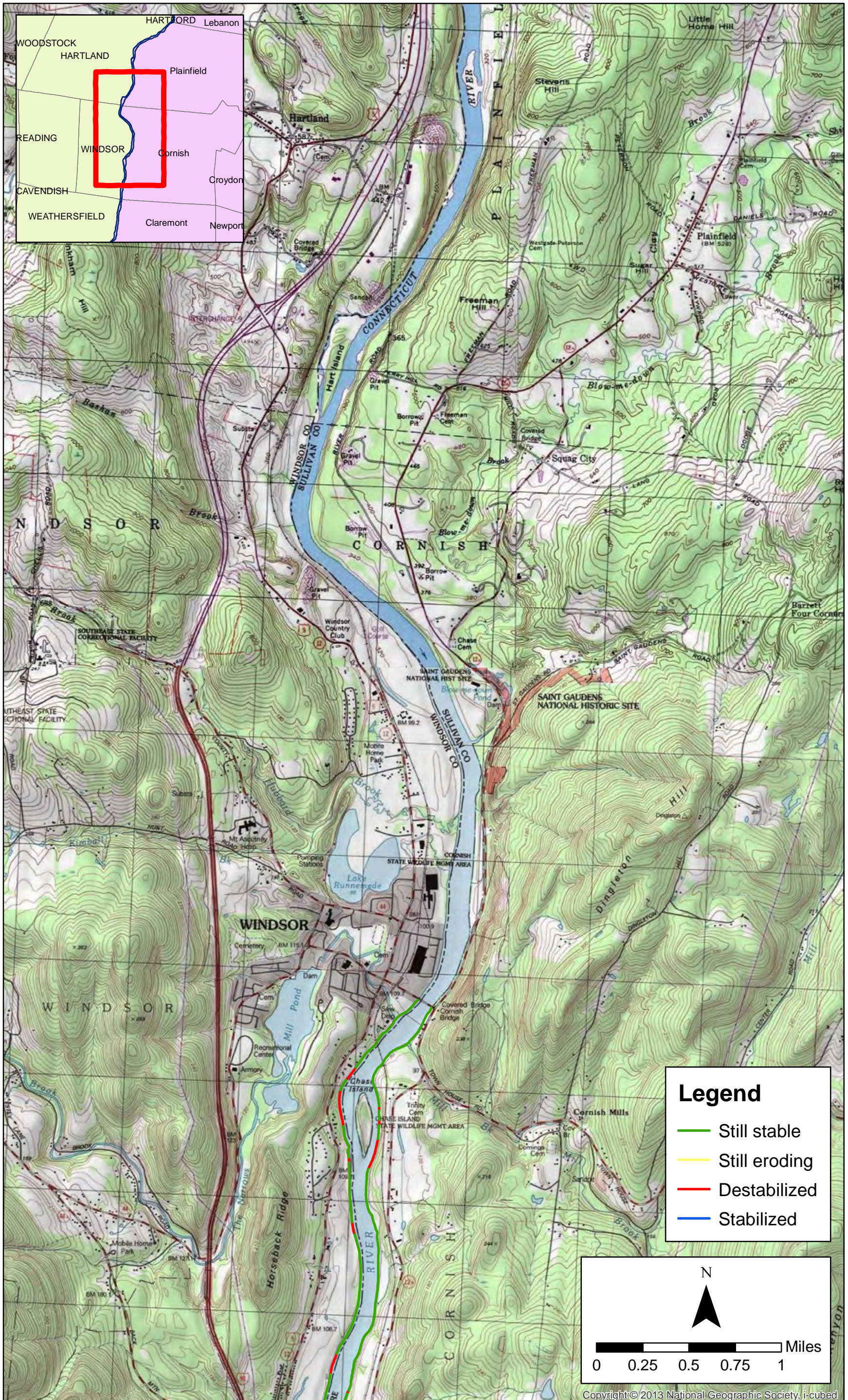


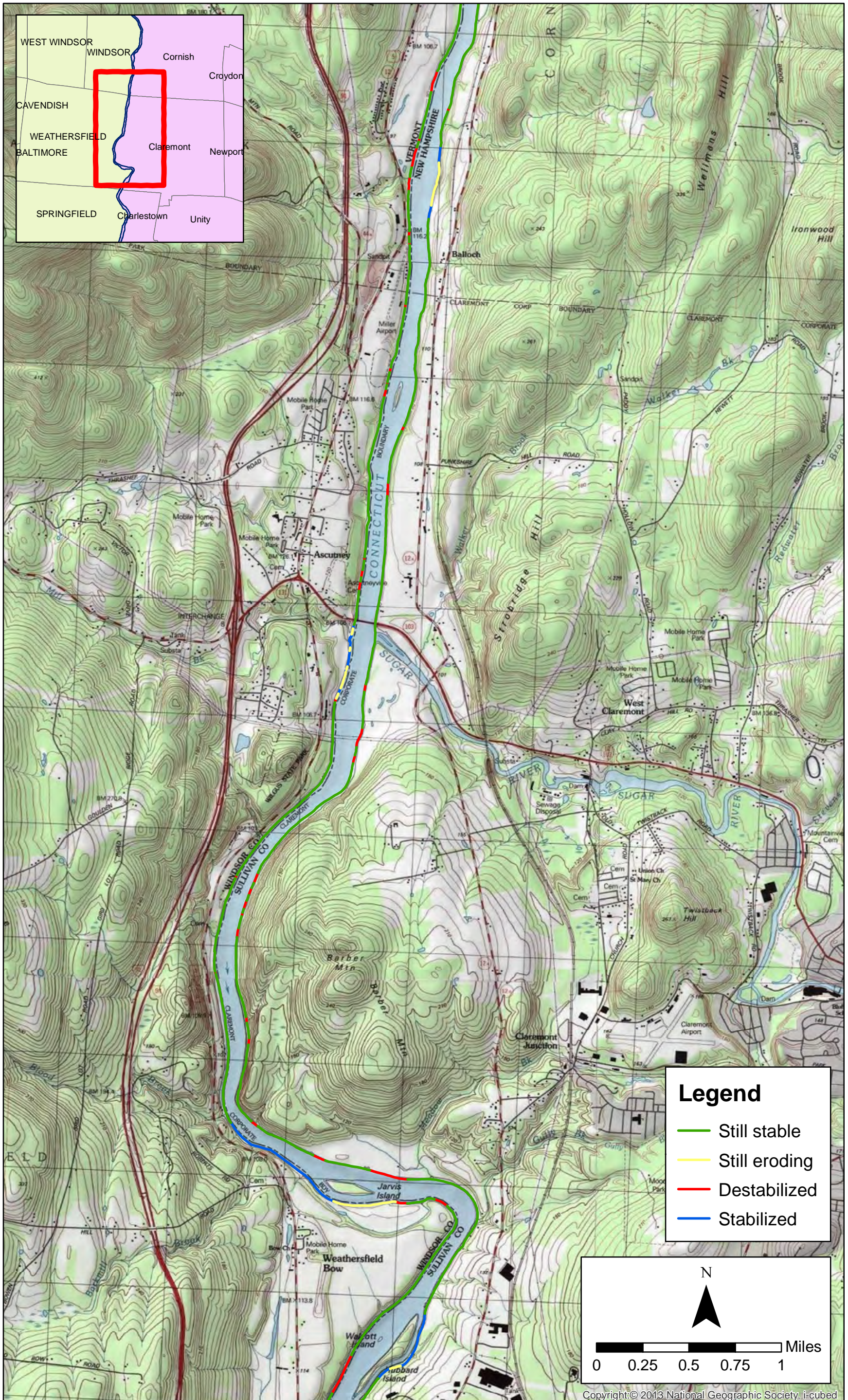


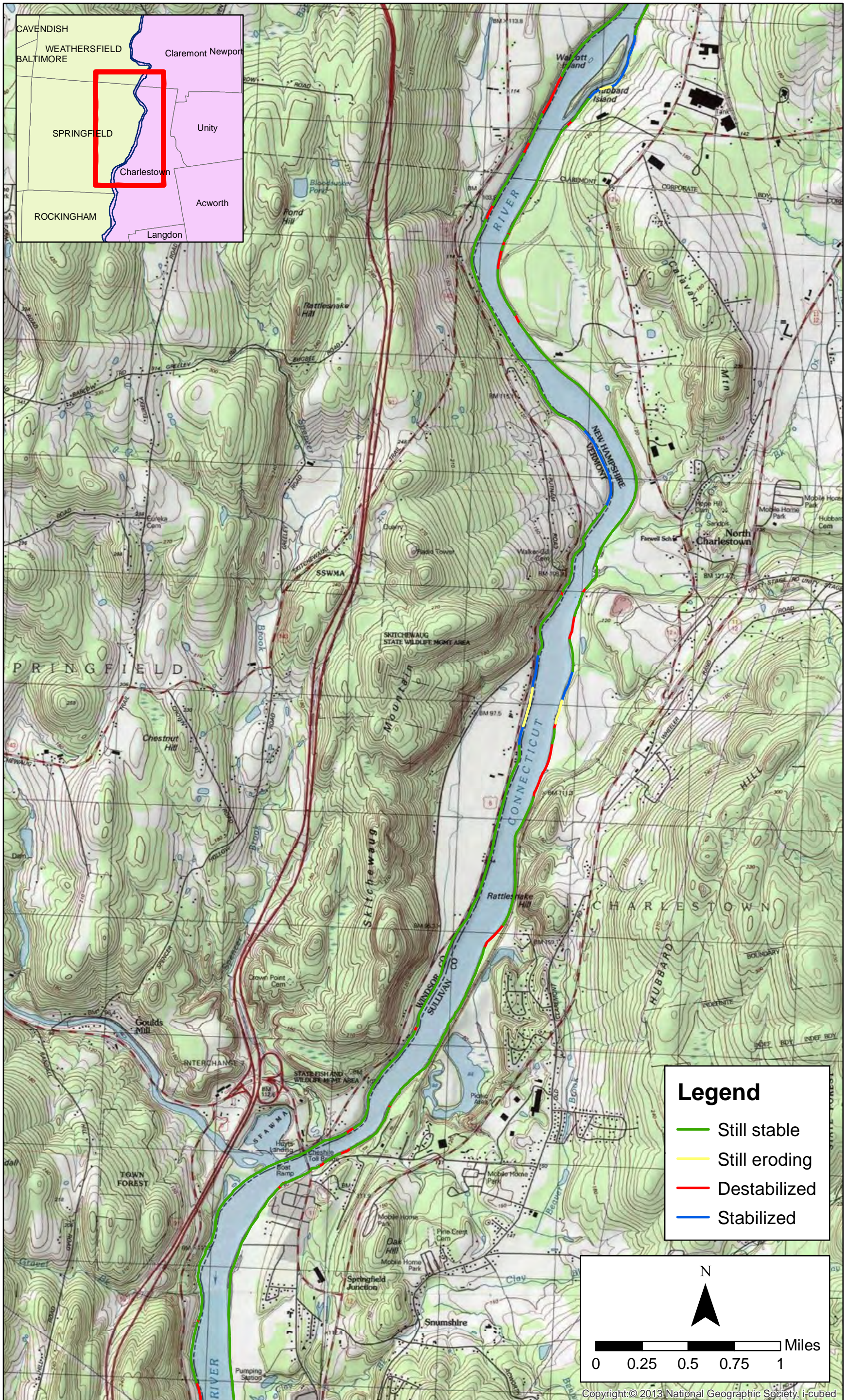


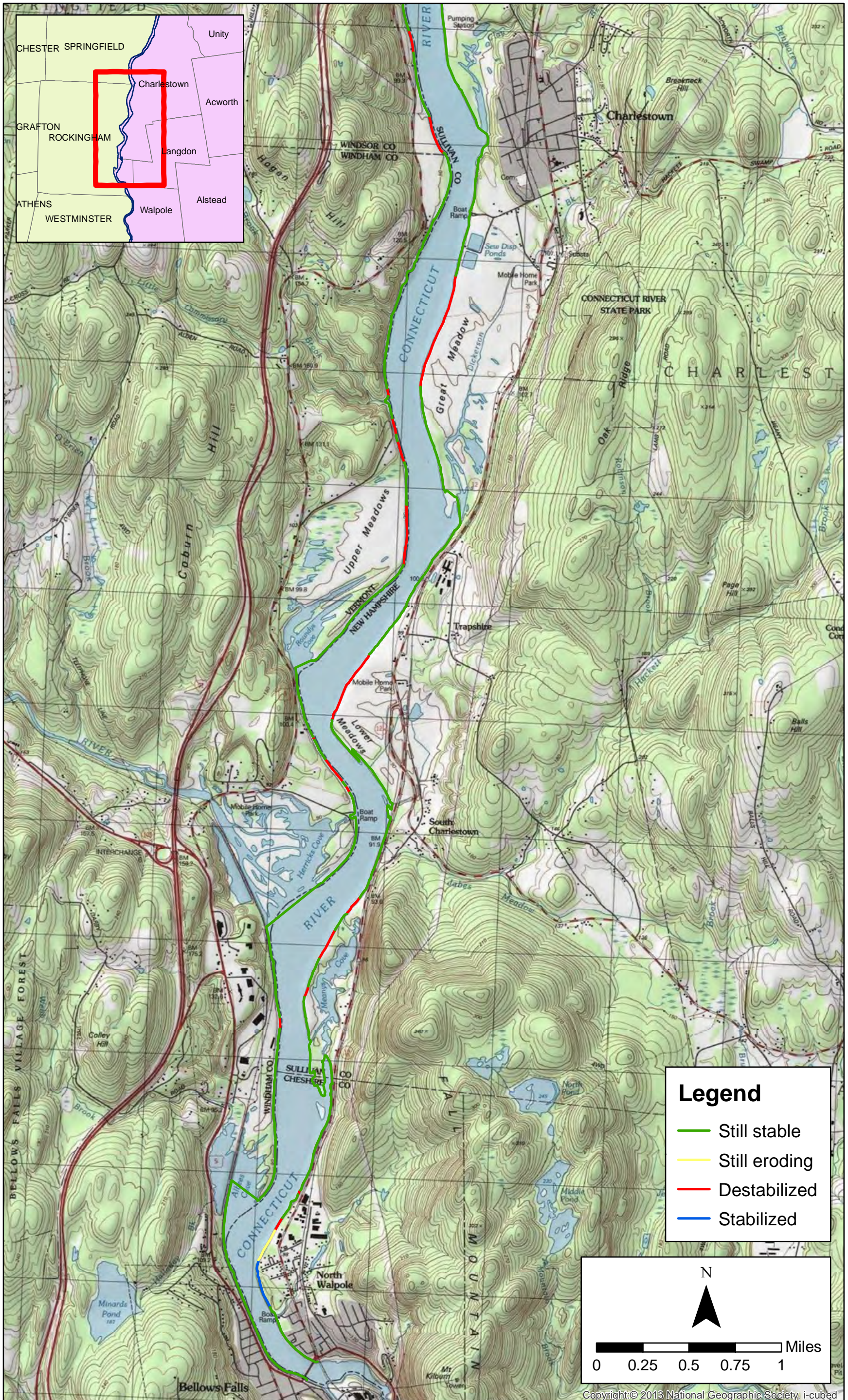
Appendix D. Comparison of 1978 and 2014 erosion. Plate 6 of 14.

Basemap imagery: USA Topo Maps.



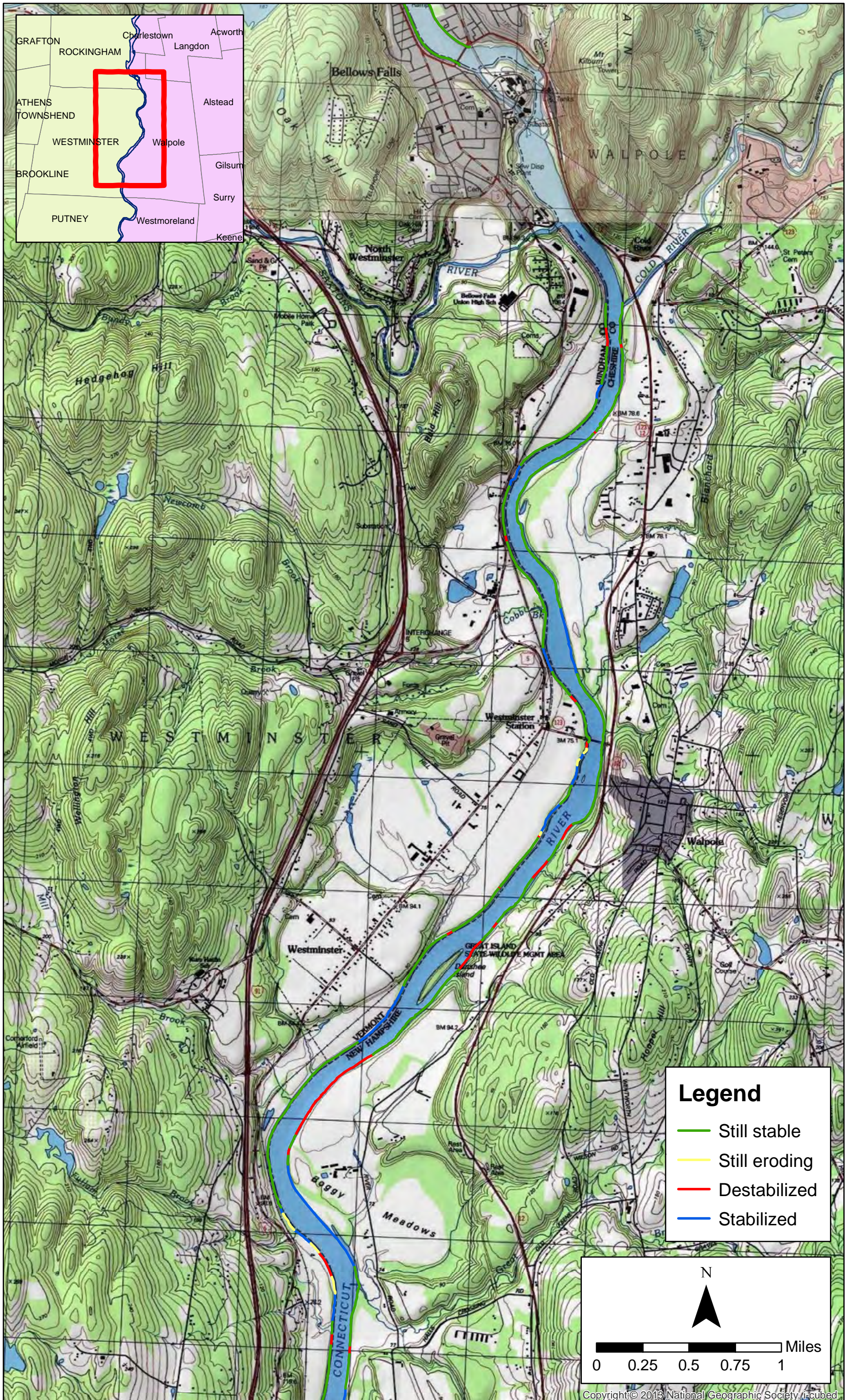


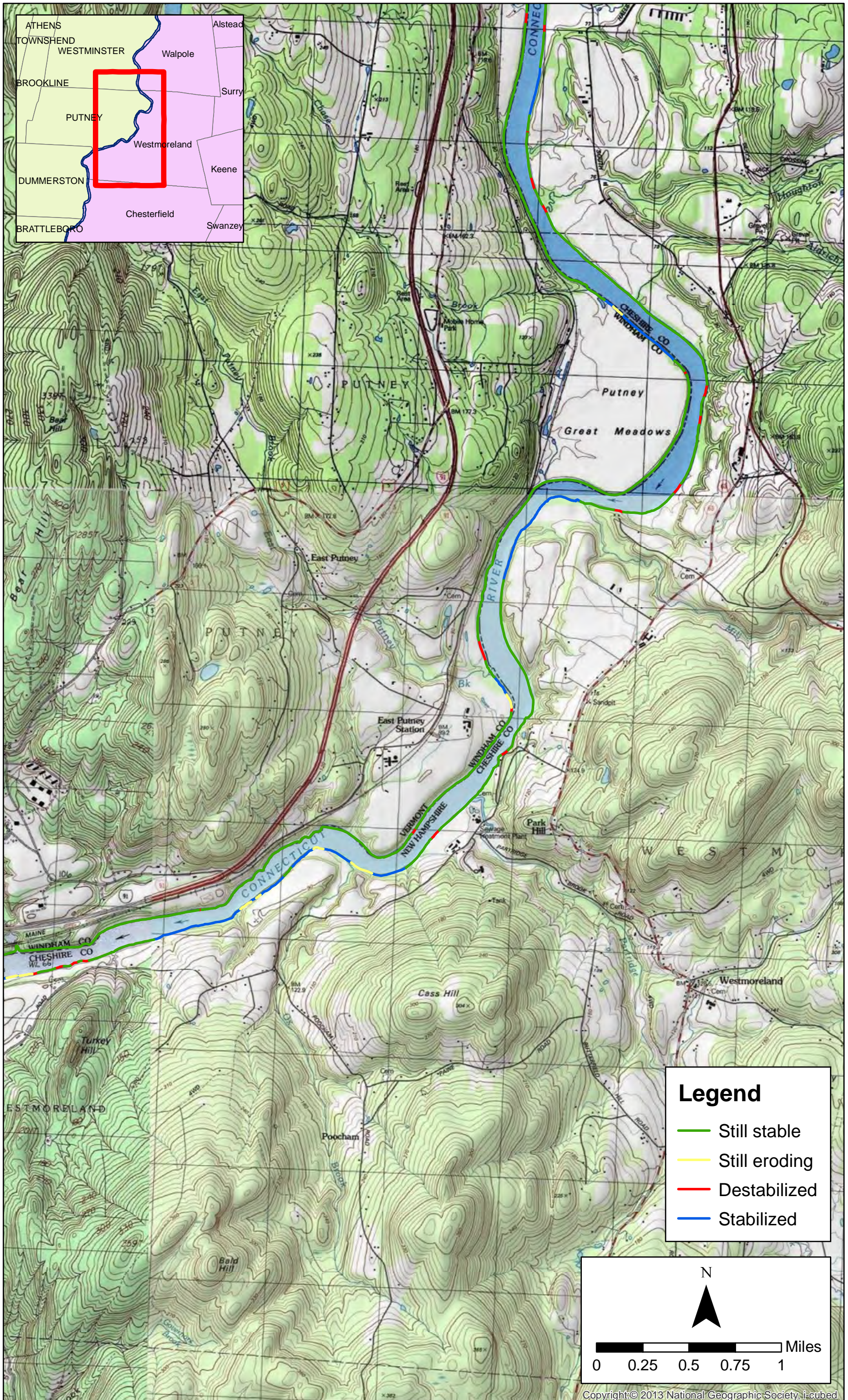


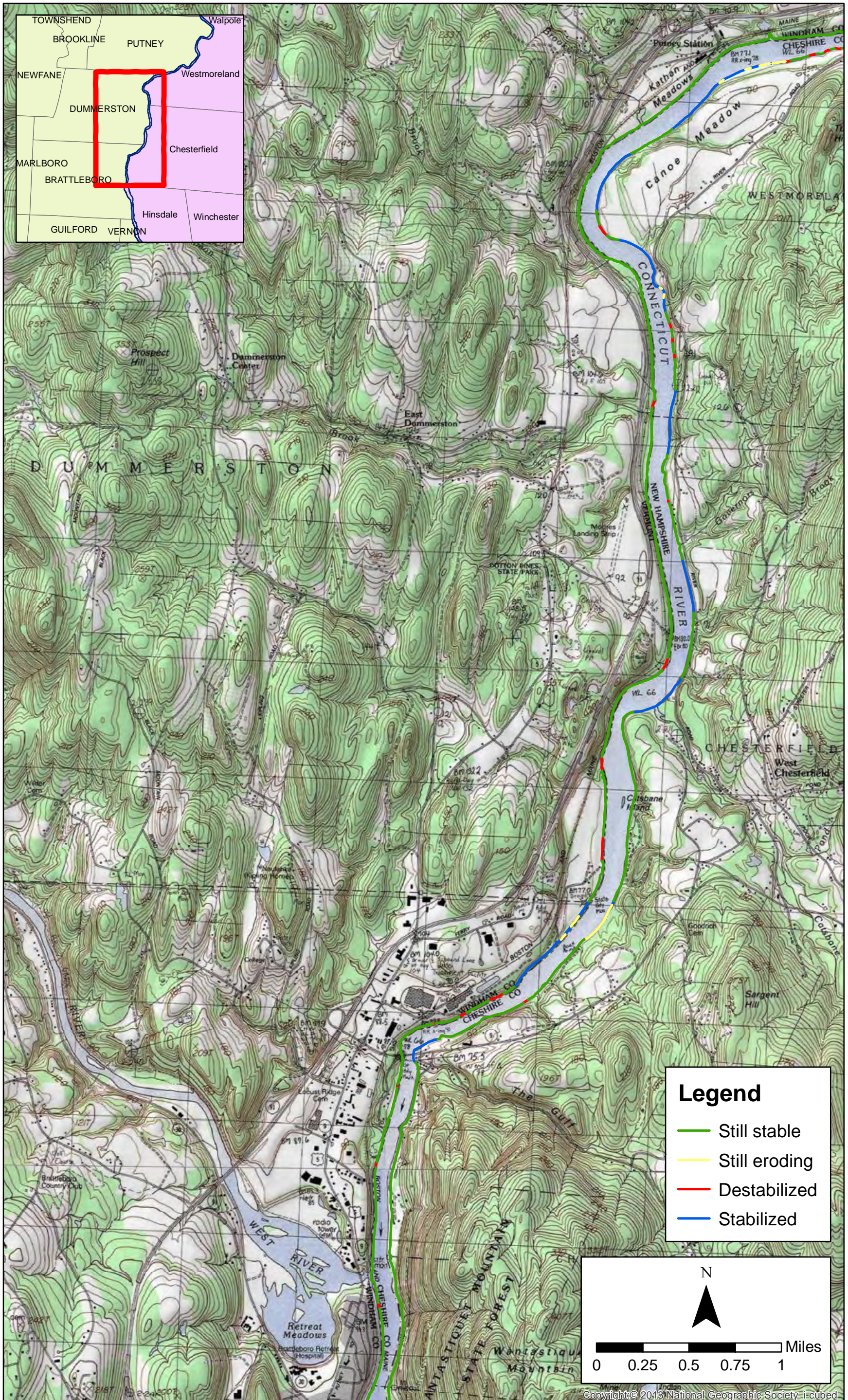


Appendix D. Comparison of 1978 and 2014 erosion. Plate 10 of 14.

Basemap imagery: USA Topo Maps.







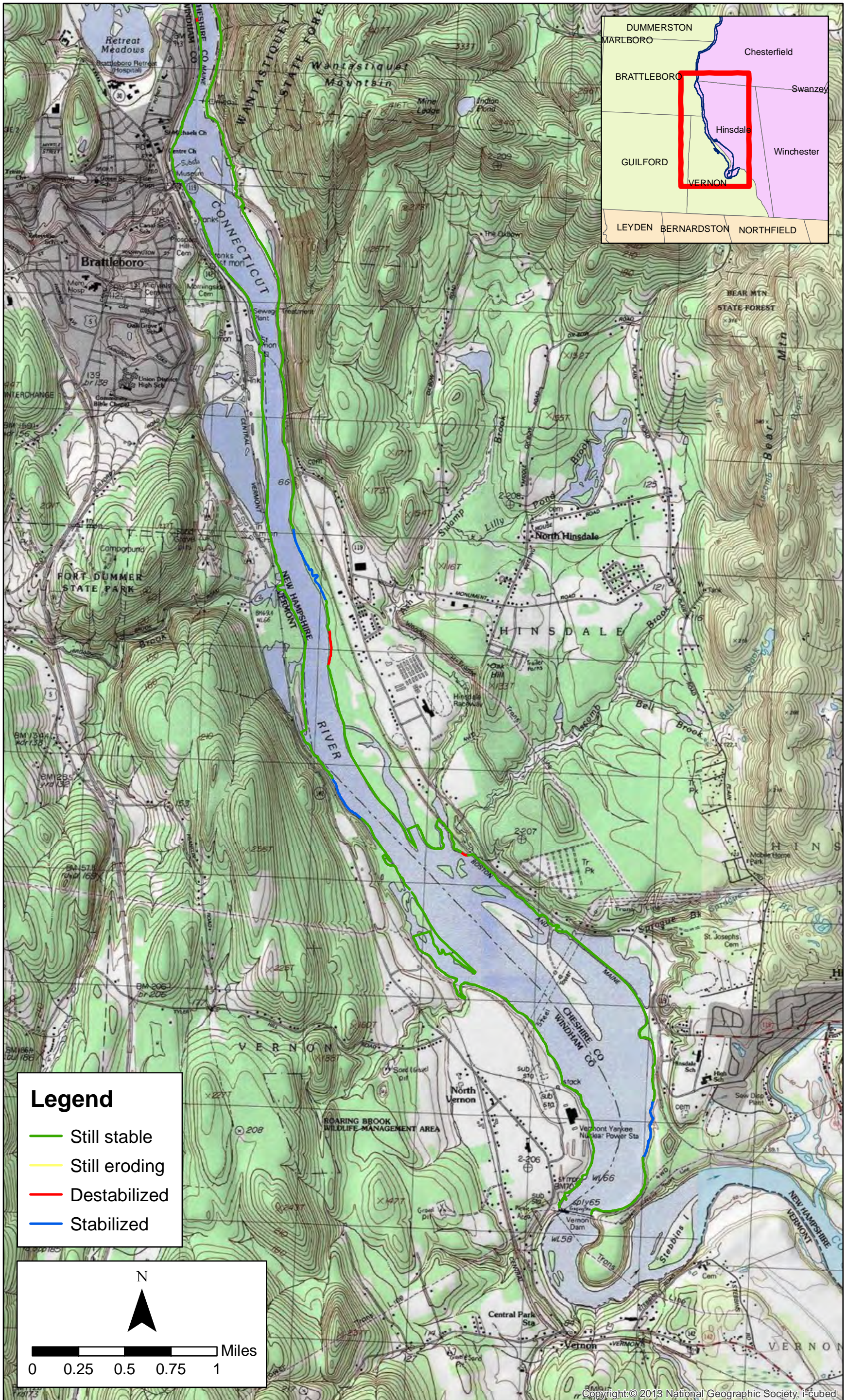
Appendix D. Comparison of 1978 and 2014 erosion. Plate 13 of 14.

Basemap imagery: USA Topo Maps.

APPENDIX E

Memo on multiple regression analysis

[This page intentionally left blank.]



Appendix E - Logistic Regression Analysis of Bank Instability

Prepared for:

Field Geology Services, LLC
Farmington ME 04938

Prepared by:

Kristian Omland, PhD
Mergus Analytics, LLC
Jericho VT 05465
komland@mergusanalytics.com

1. Summary

Instability was analyzed along both banks of a 124-mile long study area of the Connecticut River from the upper extent of the Wilder impoundment to just downstream of Vernon dam. Instability was modeled as a binary (present/absent) variable using candidate predictors of bank height, median water surface elevation (WSE) fluctuation, shear stress at the high end of project operational flows (Case 1, “low flow”), shear stress at flood flows (Case 2, “high flow” the approximate 10-yr recurrence interval), presence of armoring or forest vegetation, bend geometry (inside, outside, or straight), and the three hydropower projects (Wilder, Bellows Falls, and Vernon) in the study area. Multiple logistic regression and its extension in generalized additive models using the binomial distribution are widely used modeling strategies used to understand variation in binary variables (Venables & Ripley 2002, Wood 2005).

No predictors were very good and none explained any more than 3.5% of deviance. The richest multiple predictor model that was fit to the data only explained 8.2% of deviance, while the strongest single predictor was bank height, which explained about 3.5% of deviance whether it was modeled as a binned factor in the logistic regression framework or a continuous predictor in the generalized additive models framework. Banks lower than 10 ft were less likely to be unstable while there was a peak of instability around 20 ft of bank height. Shear stress at low flow modeled as a binned factor was the next strongest predictor, explaining 3.3% of deviance, although it did not perform as well when modeled as a continuous predictor with all the variation at low shear stress. Other variables, including median WSE fluctuation, shear stress at high flow, armoring, and bend geometry, explained relatively little deviance; presence of forest trees at the top of the bank ranked lowest. There was not a substantial amount of variability in bank instability attributable to one hydropower project over another.

Logistic regression modeling of bank instability suggested a region of higher than average bank instability for banks 20-40 ft tall; at greater median water surface elevation fluctuation levels, that region of instability expanded to higher banks. Armoring contributed a substantial additional effect, with armored banks being approximately 17% less likely to be unstable than unarmored banks when considering armored banks as a combination of those banks categorized as “armored” and “failing armor”. Beyond that, there were diminishing returns for including additional predictors. The interaction between bend geometry and armoring was examined with the data suggesting that there is greater bank instability on the inside of bends and that armoring has its greatest benefit in preventing bank instability on straight reaches.

2. Data preparation

Field Geology Services provided data in two comma-delimited text files corresponding to the left and right riverbanks. Those data were parsed, prepared, and analyzed in R (R Core Team 2016). The 1.3 million records created by segmenting the GIS shapefiles of the bank lines into points every foot along the banks provided an exhaustive estimate of the response and predictor variables for the 124-mile length of the river included in the study. The structure of the data is such that observations are not independent, a violation of one of the usual assumptions of regression. Rather, for a mapped feature that is hundreds to thousands of feet long, there are hundreds or thousands of records that are identical in terms of bank instability and all candidate predictor variables. Nonetheless, the models used here are useful for computing empirical estimates from the data, particularly through smoothing and estimation of additive effects and/or interactions.

The unique identifier provided with each record was modified by prefixing either L for left or R for right bank using as many as five leading zeros. With record identifiers constructed that way (i.e., L000001 through R667759), it was possible to combine the data from the left and right banks while retaining an identifier that could be used to locate records in the original data files.

Bank instability was recoded as a binary variable: 1 for unstable and 0 for stable.

The candidate predictor, armored (present/absent), was extracted from the Stability_ field with values 1-4 being un-armored while values 5-6 were armored (i.e., armored and failing armor). Forested (Y/N) was interpreted from the Buffer_Cat field with 1 referring to mature trees as determined from remote sensing data and 0 referring to any other condition (agriculture, shrubland, marsh, etc.). Bend was recoded for convenience with 0 referring to straight reaches but using -1 (rather than 1) to indicate inside and 1 (rather than 2) to indicate the bank on the outside of a bend.

Binned representation of bank height and median WSE fluctuation were constructed following quantiles (cutpoints) used in the original study report. Binned representation of shear stress was constructed based on ranks to populate ten approximately equally populated deciles.

3. Logistic regression models of bank instability

All models described here are essentially logistic regression models in the Generalized Linear Models (GLM) framework with bank instability (1 unstable, 0 stable) modeled using a binomial distribution and Shape_Leng applied as a weight (Shape_Leng was 1 for 96.6% of observations but took on values between 0.01 and 1.01).

With no predictors (intercept-only model), probability of bank instability was 39.7%, representing the percentage of banks mapped as unstable.

Confidence intervals about the estimates are not reported for two reasons. First, conceptually with a foot-by-foot census of both banks of the 124-mile study area, there has been no sampling and there is no sampling error to be estimated. Second, in practical terms the confidence intervals estimated from a data set of over 1 million records are so narrow as to be uninformative.

Candidate predictor variables were bank height, median WSE fluctuation (fluctuation), shear stress (independently at low and high flows, averaged across full channel width), presence of armoring or forest vegetation, and bend geometry (inside, outside, or straight). The three hydroelectric projects were optionally included as a covariate to investigate whether the effect of

the other predictors differed in areas influenced by the three projects. For the continuous predictors of bank height, fluctuation, and shear stress, models were fit using the variables as binned factors in logistic regression or as smooth predictors in the generalized additive models (GAM) framework.

3.1. Single Predictors

Models with single predictors were fit using either GLM (Table 1) or GAM (Table 2). Typically, model selection is an optimization problem balancing complexity (the number of estimated parameters) and fit. However, with over 1 million records, these data support estimation of models of virtually unlimited complexity. However, there are diminishing returns in terms of improving fit: the best single-predictor models explain about 3.5% of null deviance while models with multiple factors do not improve that much. Furthermore, the cost of increasingly complex models is difficulty in interpretation. For this analysis, rather than relying on an automated model selection process, model complexity was gradually increased starting with the best single-predictor model and adding terms one-by-one until model fit and interpretability seem balanced.

Table 1. Logistic regression models using single factor predictors (continuous variables binned). Intercept-only model in first row (1 estimated parameter). Degrees of freedom (df) are the number of estimated parameters; deviance is a measure of model fit (lower values reflect better fit; deviance can be interpreted in a similar way to residual sum of squares in ordinary linear models). Other models listed in decreasing order of model fit. Percentage deviance explained is the decrement from the intercept-only model [e.g., with 1,759,429 the deviance of the intercept-only model, the model that includes bank height diminishes deviances by 3.525% ($(1,759,429 - 1,697,407) / 1,759,429 = 3.525\%$).]

Model	df	Deviance	% deviance explained
(intercept)	1	1,759,429	NA
Bank height (bins)	9	1,697,407	3.525
Shear stress, low flow (bins)	10	1,700,709	3.337
Fluctuation (bins)	14	1,739,493	1.133
Shear stress, high flow (bins)	10	1,743,720	0.893
Armored	2	1,747,416	0.683
Bend geometry	3	1,755,146	0.243
Project	5	1,757,864	0.089
Forested	2	1,758,926	0.029

Table 2. GAM models using continuous single factor predictors. Model deviance may be compared to the intercept-only model in Table 1.

Model	df	Deviance	% deviance explained
Bank height	4.99	1,698,417	3.468
Shear stress, low flow	4.96	1,739,895	1.110
Shear stress, high flow	4.97	1,744,550	0.846
Fluctuation	4.92	1,756,019	0.194

3.1.1. Bank Height

Bank height had been divided into nine approximately equally-populated bins for the original study report (Table 3). Probability of bank instability was lower than average for banks less than 5 ft high and higher than average for banks between 15 and 30 ft high; for banks higher than 30 ft, instability was close to average (Figure 1). There does not appear to be a linear relationship between bank height (or any transformation of bank height) and instability, therefore the relationship was modeled in a GAM using a flexible functional form (tensor product). Using the cutpoints between bins as knots for the fitted GAM (8 knots), the general pattern of low instability on low banks and greatest instability on banks 15-25 ft high is reinforced. Permitting the curve-fitting software to select the complexity of the smooth curve automatically, only 5 knots were supported, which is a simpler and smoother model, but the interpretation remains similar with below-average bank instability on banks less than 6 ft high and peak instability on banks about 20 ft high (± 5 ft.; Figure 2)

Table 3. Proportion of riverbank in each bank height bin that is unstable, and ratio of that proportion to the overall proportion, 0.397 (i.e., the 39.7% of the banks that are unstable). Where the erosion ratio is less than 1, the proportion unstable is less than the overall proportion, and vice versa.

Bin	Realized Range		N	Proportion Unstable	Erosion Ratio
$y < 1$	-2.1	0.9	69,305	0.155	0.39
$1 \leq y < 5$	1	4.9	119,443	0.177	0.45
$5 \leq y < 8$	5	7.9	94,112	0.393	0.99
$8 \leq y < 10$	8	9.9	98,317	0.361	0.91
$10 \leq y < 15$	10	14.9	256,793	0.415	1.05
$15 \leq y < 20$	15	19.9	222,054	0.488	1.23
$20 \leq y < 30$	20	29.9	202,898	0.497	1.25
$30 \leq y < 50$	30.1	49.8	161,975	0.409	1.03
$y \geq 50$	50	97.4	107,608	0.390	0.98

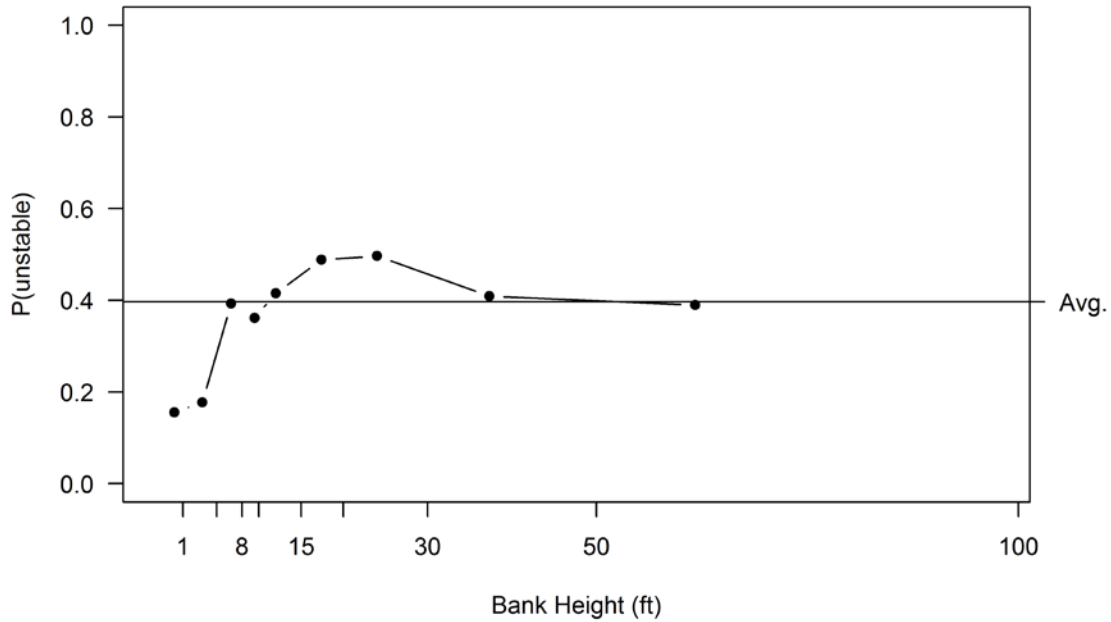


Figure 1. Probability of bank instability by binned bank height; the realized median within each bin is used to fix the x-axis value of each point. Overall average indicated by horizontal line.

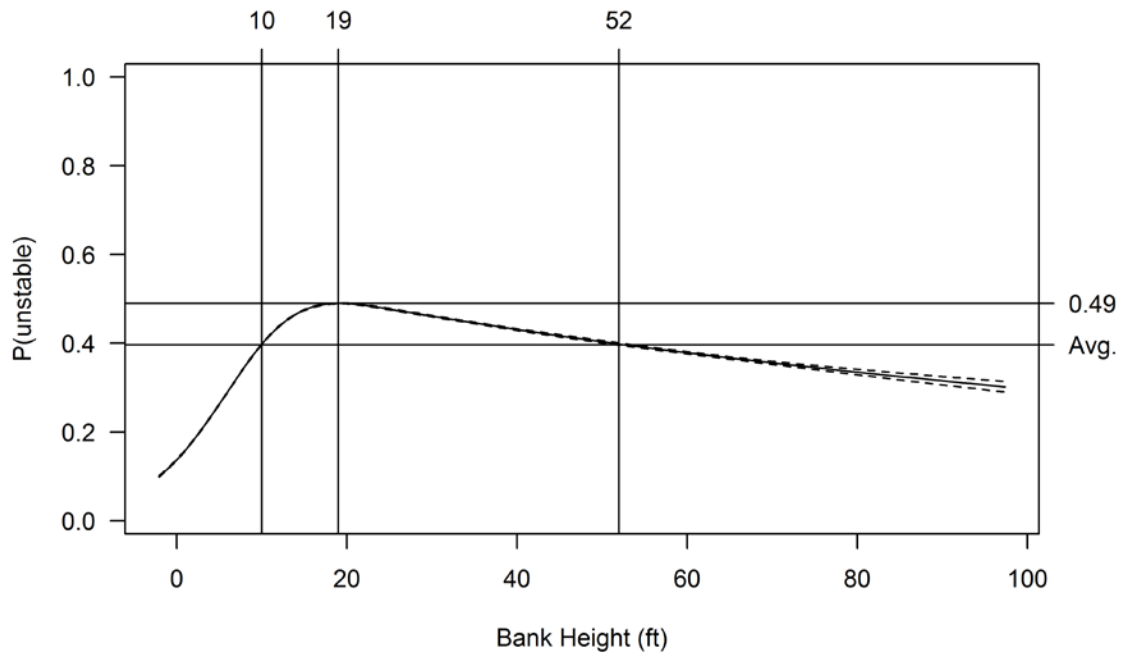


Figure 2. Smooth (tensor product) model of the relationship between bank height and bank instability. Extra lines and axis labels added for interpretability. Instability is below average for banks lower than 10 ft. (or higher than 52 feet) and peaks at 49% for banks around 19 ft. high.

3.1.2. Median Water Surface Elevation Fluctuation

Median WSE fluctuation (fluctuation) ranged from less than 1 ft to over 7 ft (in riverine reaches) but more than 71% of the banks in the study area had a median fluctuation range of < 1.5 ft. Instability ranked highest in bins representing fluctuations 3-3.5 ft, 1.5-2 ft, and 5.5-6 ft; it ranked lowest in bins 6-6.5 ft, over 7 ft, and 4.5-5 ft (Table 4, Figure 3). Cutting the range into deciles (with the first 7 deciles all squeezed into 0.67-1.4 ft) did not make for a more regular or interpretable result. Fitting a GAM (tensor product) to the data resulted in a model with a hump around 2.25 ft, but overall little variation is observed over the range of fluctuation (Figure 4).

Table 4. Proportion of riverbank in each fluctuation bin that is unstable and ratio of that proportion to the overall proportion, 0.397. Where the erosion ratio is less than 1, proportion unstable is less than the overall proportion, and vice versa.

Bin	Realized Range		N	Proportion Unstable	Erosion Ratio
$y < 1$	0.67	0.99	295,751	0.427	1.08
$1 \leq y < 1.5$	1.00	1.49	650,504	0.374	0.94
$1.5 \leq y < 2$	1.50	1.99	65,911	0.525	1.32
$2 \leq y < 2.5$	2.00	2.49	39,523	0.459	1.16
$2.5 \leq y < 3$	2.50	2.99	19,294	0.437	1.10
$3 \leq y < 3.5$	3.00	3.49	31,707	0.563	1.42
$3.5 \leq y < 4$	3.50	3.99	36,012	0.376	0.95
$4 \leq y < 4.5$	4.00	4.49	40,670	0.353	0.89
$4.5 \leq y < 5$	4.50	4.99	66,286	0.295	0.74
$5 \leq y < 5.5$	5.00	5.49	26,874	0.319	0.80
$5.5 \leq y < 6$	5.50	5.99	36,694	0.506	1.28
$6 \leq y < 6.5$	6.00	6.49	9,447	0.159	0.40
$6.5 \leq y < 7$	6.50	6.99	11,955	0.313	0.79
$y \geq 7$	7.00	7.10	1,877	0.241	0.61

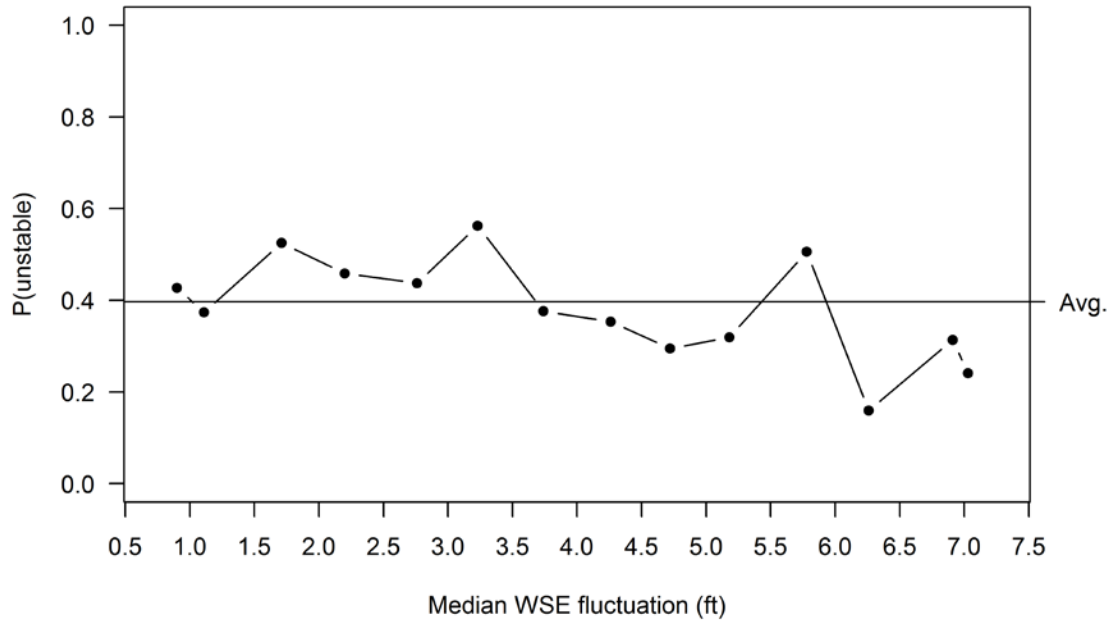


Figure 3. Probability of bank instability by binned fluctuation; the realized median within each bin is used to fix the x-axis value of each point. Overall average indicated by horizontal line.

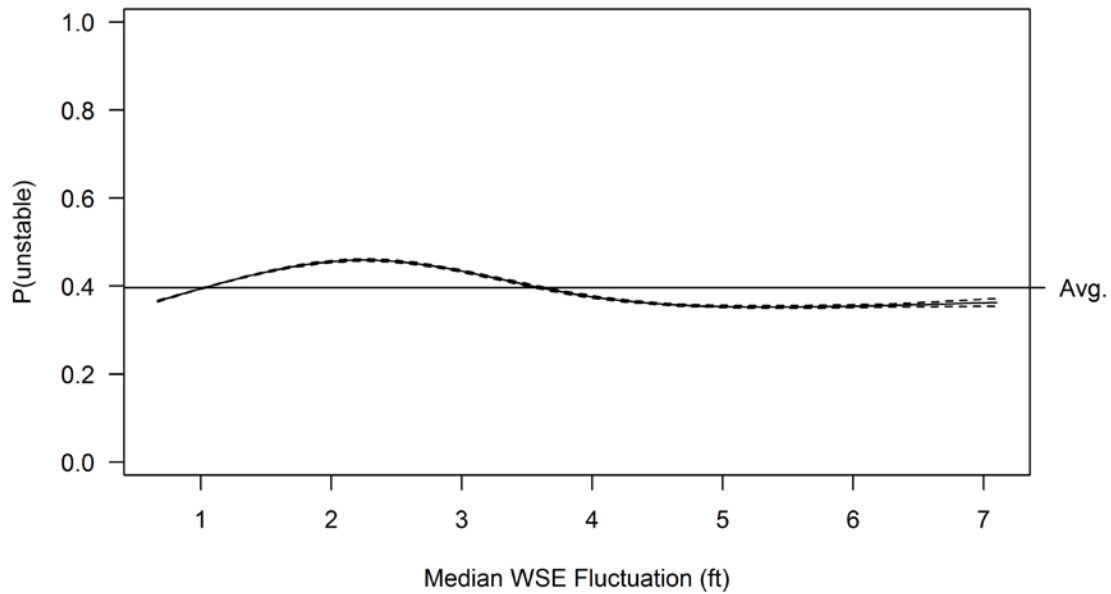


Figure 4. Smooth (tensor product) model of the relationship between fluctuation and bank instability.

3.1.3. Shear Stress

Estimated shear stress at “Case 1” operational flows (Case 1 condition was taken as the discharge at the upper end of the project’s operating range, channel-wide average) was 0 pounds per square foot (psf) for 80,652 records and was as high as 6.29 psf in the riverine section just below Bellows Falls dam. Records were assigned to approximate deciles based on Case 1 flow shear stress although, because of limited precision, bins could not be equally populated (Table 5). Instability was below average where shear stress at the Case 1 flow was less than 0.02 psf. Instability appeared more prevalent where Case 1 flow shear stress was between 0.02 and 0.2 psf (Figure 5).

Estimated shear stress at “Case 2” high flows (Case 2 condition was taken as the approximate 10-year recurrence interval, channel-wide average) ranged from 0.01 to 15.63 psf. Bank instability was close to average across most of that range (Table 6, Figure 7).

When GAMs were fit to Case 1 and Case 2 shear stress data, both models were dominated by a tail of no instability above a certain shear stress level (Figure 6, Figure 8). For Case 1 flow conditions, there were no instances of unstable bank where shear stress was greater than 1.52 psf (represented by 5,361 records). For Case 2 high flow conditions, there was no bank instability where shear stress was greater than 1.413 psf (5,083 records).

Table 5. Proportion of riverbank in each Case 1 operational flow shear stress bin that is unstable and ratio of that proportion to the overall proportion, 0.397. Where the erosion ratio is less than 1, Proportion unstable is less than the overall proportion, and vice versa.

Bin	Realized Range		N	Proportion Unstable	Erosion Ratio
1	0	0.0099	103,582	0.215	0.54
2	0.01		247,927	0.274	0.69
3	0.0101	0.0199	34,074	0.293	0.74
4	0.02		211,483	0.418	1.05
5	0.0201	0.0299	39,645	0.450	1.14
6	0.03	0.0399	130,120	0.529	1.33
7	0.04	0.0546	165,943	0.493	1.24
8	0.0547	0.0799	130,540	0.483	1.22
9	0.08	0.1299	135,946	0.474	1.19
10	0.13	6.29	133,245	0.329	0.83

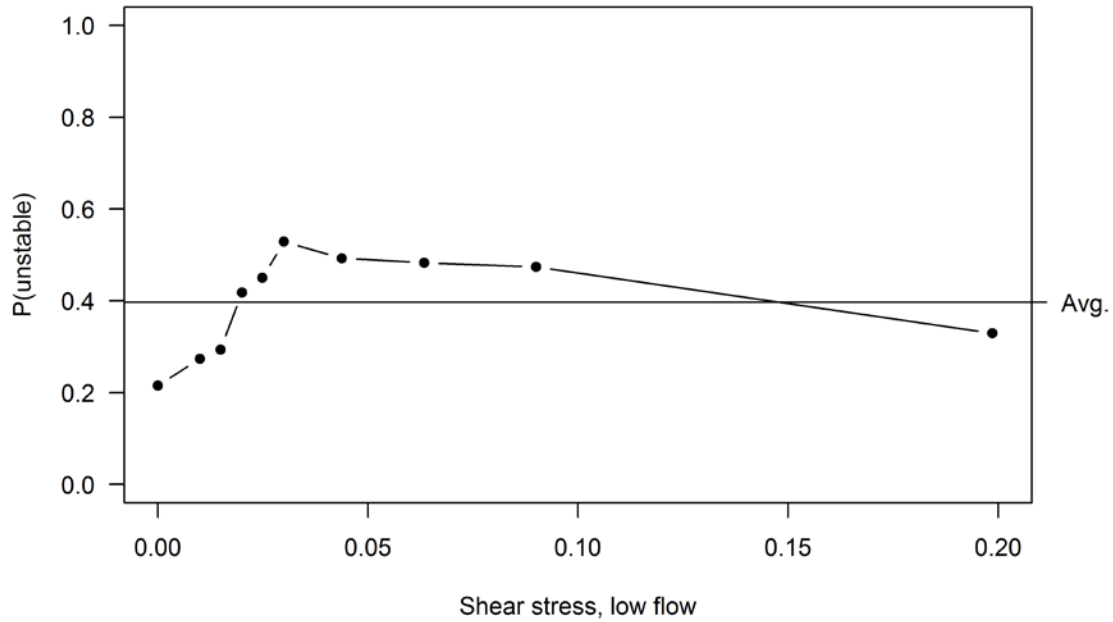


Figure 5. Probability of bank instability by binned shear stress in Case 1 operational flow conditions; the realized median within each bin is used to fix the x-axis value of each point; note the compressed x-axis compared to Figure 6. Overall average indicated by horizontal line.

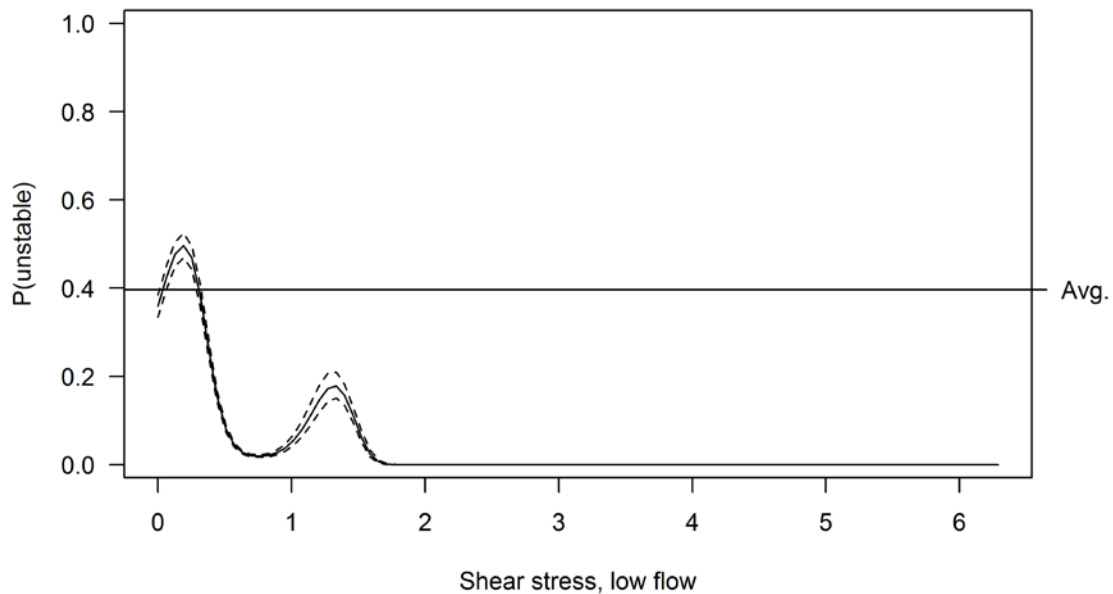


Figure 6. Smooth (tensor product) model of the relationship between shear stress (Case 1 operational flow; note the expanded x-axis compared to Figure 5) and bank instability.

Table 6. Proportion of riverbank in each Case 2 high flow shear stress bin that is unstable and ratio of that proportion to the overall proportion, 0.397. Where the erosion ratio is less than 1, the proportion unstable is less than the overall proportion, and vice versa.

Bin	Realized Range		N	Proportion Unstable	Erosion Ratio
1	0.01	0.05	141,742	0.462	1.17
2	0.0501	0.08	138,194	0.371	0.93
3	0.0801	0.1099	110,893	0.370	0.93
4	0.11	0.1299	126,560	0.393	0.99
5	0.13	0.1491	148,739	0.399	1.01
6	0.1492	0.17	147,954	0.434	1.09
7	0.1701	0.2045	118,647	0.431	1.09
8	0.2046	0.25	138,485	0.441	1.11
9	0.2501	0.3499	125,958	0.388	0.98
10	0.35	15.63	135,333	0.266	0.67

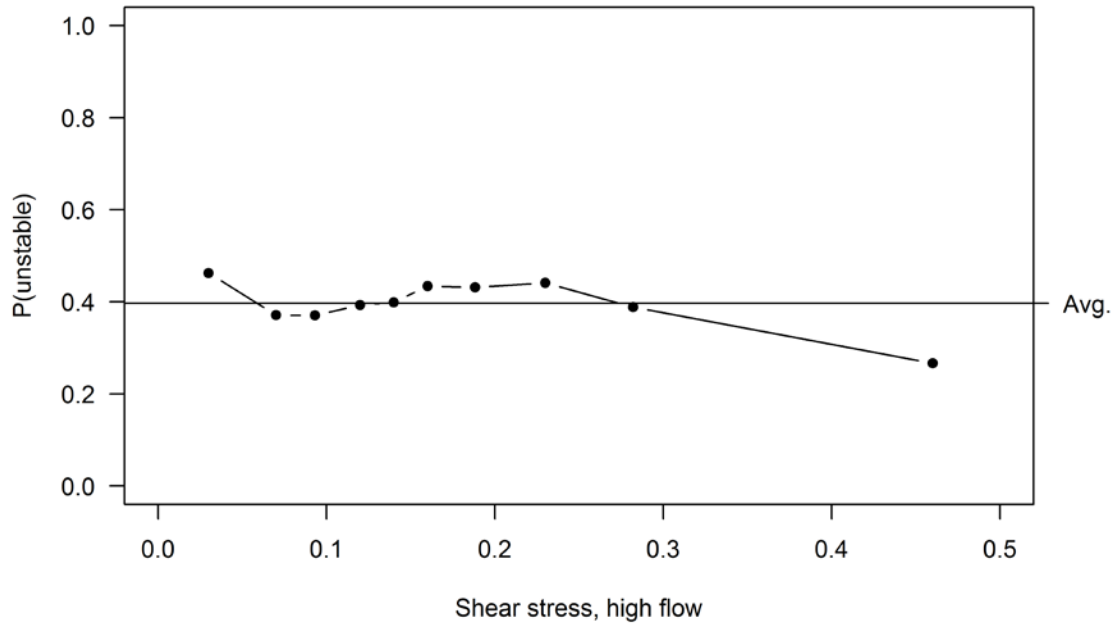


Figure 7. Probability of bank instability by binned shear stress in Case 2 high flow conditions; the realized median within each bin is used to fix the x-axis value of each point; note the compressed x-axis compared to Figure 8. Overall average indicated by horizontal line.

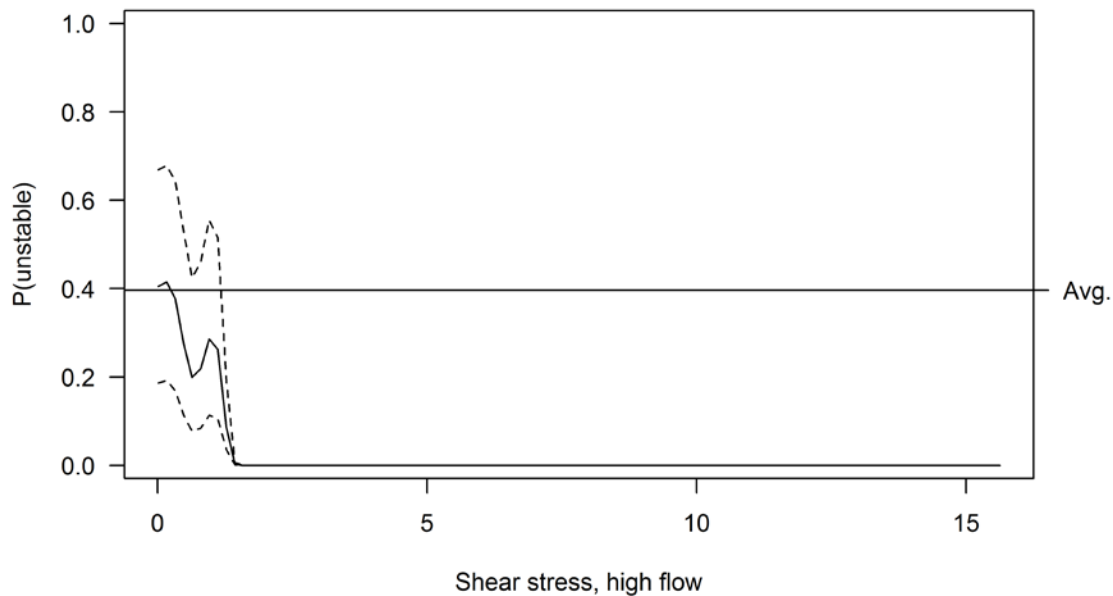


Figure 8. Smooth (tensor product) model of the relationship between shear stress (Case 2 high flow; note the expanded x-axis compared to Figure 7) and bank instability.

3.1.4. Other Factors

- Unarmored banks (the large majority of the study area) had somewhat higher than average instability: 42.0%. In contrast, armored banks had only 30.7% instability.
- Straight sections had 42.1% instability. Insides of bends had 40.5% while the outside of bends had 35.6% instability.
- Forested banks had 40.1% instability while unforested banks had 37.6% instability.
- Bank instability varied little between the three hydropower projects. Bank instability was only 34.5% in the Bellows Falls riverine section (given the long length of bedrock immediately downstream of the dam) but elsewhere bank instability was close to the study area average of 39.7%.

3.2. Multiple Predictors

3.2.1. Maximizing goodness of fit using GAMS

Beginning with the single-predictor model that explained the most deviance, other factors were considered in addition, to better explain the deviance. Bank height explained about 3.5% of bank instability, whether using it as a binned factor or a continuous predictor in a GAM. Adding shear stress during Case 1 flow or WSE fluctuation to the GAM increased deviance explained to 5.96% and 4.93%, respectively; and adding armor as a third variable increased that quantity to 7.13% and 6.45%, respectively (Table 7). Adding bend geometry as a fourth variable increased the percent deviance explained to 7.39% and 6.75%, respectively, representing diminishing returns for added model complexity given the limited increase in the percent deviance explained.

Models adding Case 1 flow shear stress are uninformative because they are dominated by two features (Figure 9). First, all the instability is depicted in the narrow region where shear stress is low, therefore there is virtually no resolution on how instability changes as shear stress increases. Second, all of the instances of shear stress being greater than 1.5 psf (at Case 1 flow) are along banks that are 7.9, 37.3, or 49.3 ft high, therefore the low estimates for the highest shear stresses for Case 1 flow conditions at other bank heights reflect a lack of data rather than bank stability.

The model including WSE fluctuation in addition to bank height depicts a ridge of higher than average bank instability on banks around 20-40 ft. high that flares out as WSE fluctuation increases (Figure 10). The effect of armoring is modeled as an overall average adjustment, which lowers the probability of instability by 17%.

The model adding bend geometry increased the percent deviance explained only to 6.75%, again representing diminishing returns, with a contour plot of the results suggesting no different interpretation.

Table 7. GAM models using numerous continuous factor predictors and/or factors. Model deviance may be compared to the intercept-only model in Table 1 and Table 2. Bank height and WSE fluctuation were modeled allowing the algorithm to automatically select the knots rather than using the cutpoints from the original study report.

Model	df	Deviance	% Deviance Explained
Bank Height	4.99	1,698,417	3.47
Bank Height, shear-low (Case 1 flow)	21.99	1,654,581	5.96
Bank Height, shear-low (Case 1), armored	22.97	1,633,957	7.13
Bank Height, shear-low (Case 1), armored, bend	24.96	1,629,480	7.39
Bank Height, fluctuation	24.88	1,701,352	4.93
Bank Height, fluctuation, armored	25.83	1,674,089	6.45
Bank Height, fluctuation, armored, bend	27.74	1,668,668	6.75

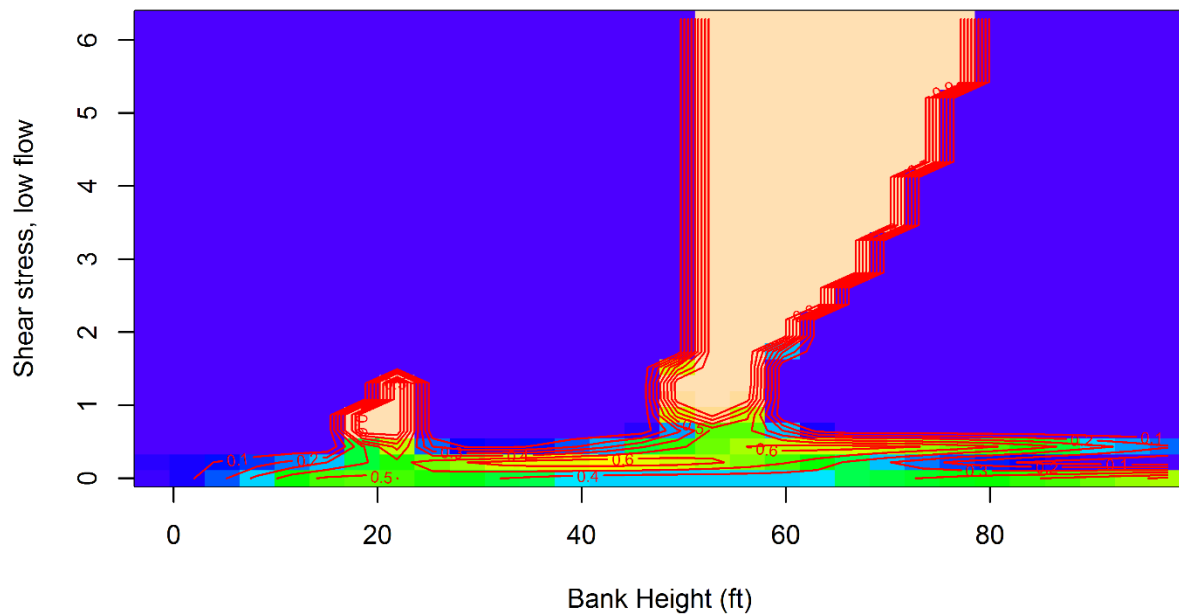


Figure 9. Contour plot of a fitted GAM with bank height (x -axis) and shear stress at Case 1 flow (y -axis) modeled as continuous predictors (tensor product). Labeled contour lines delimit regions with more than the specified probability of bank instability. The extensive purplish-blue regions were largely unobserved (e.g., no banks taller than 37.3 feet with more than 1.52 psi shear stress).

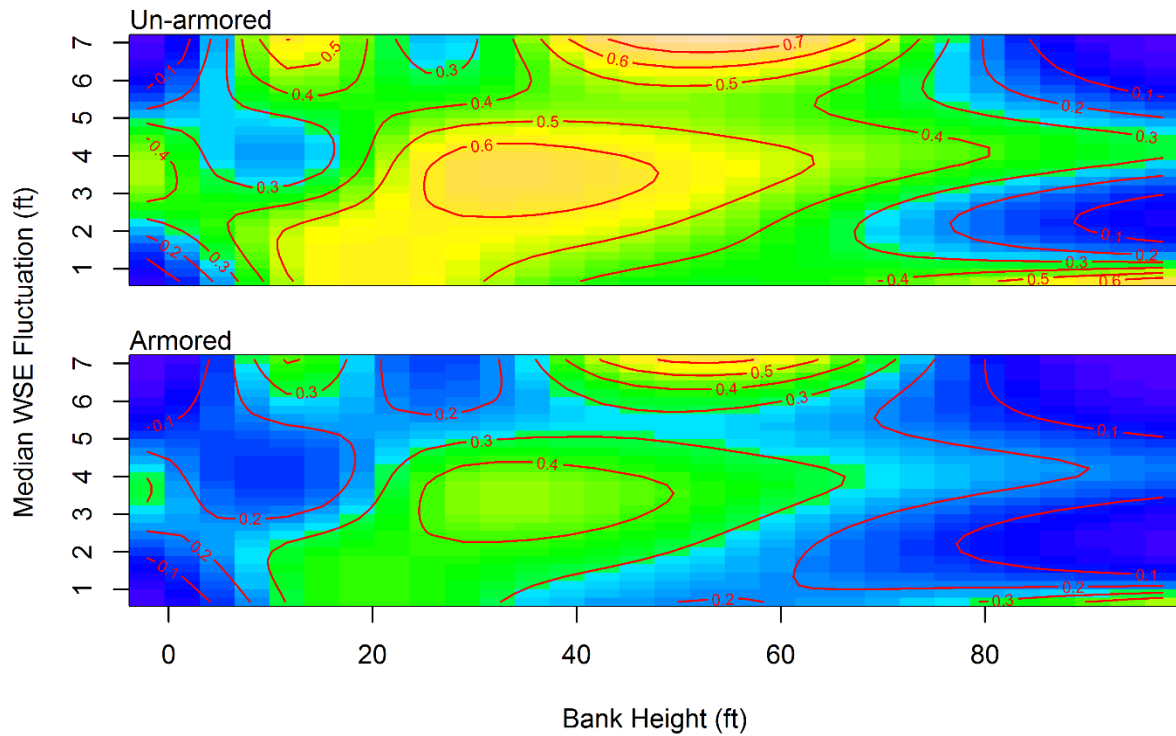


Figure 10. Contour plots of a fitted GAM with bank height (x -axis) and WSE fluctuation (y -axis) modeled as continuous predictors (tensor product) and armoring a factor (top panel un-armored, bottom panel with armor). Labeled contour lines delimit regions with more than the specified probability of bank instability.

3.2.2 Maximizing goodness of fit using logistic regression

Using an automated model selection routine (stepAIC, Venables & Ripley 2002), a model was fit using all seven variables additively (binned continuous variables: bank height, WSE fluctuation, shear stress at Case 1 flow, shear stress at Case 2 high flow; and factors: bend, armored, forested). The routine adds terms sequentially that most improve model fit. The first three terms added (i.e., those that most improved model fit) were bank height, shear stress during Case 1 flow events, and WSE fluctuation. As terms were added, the residual deviance declined, but with diminishing returns. At the end of the sequence, adding forested bank as a predictor diminished residual deviance from 1,616,250 to 1,615,963, which improved the percent deviance explained only from 8.138% to 8.154% (Figure 11). In this and other efforts, no statistical model of the data was found that could explain more than about 8.2% of deviance.

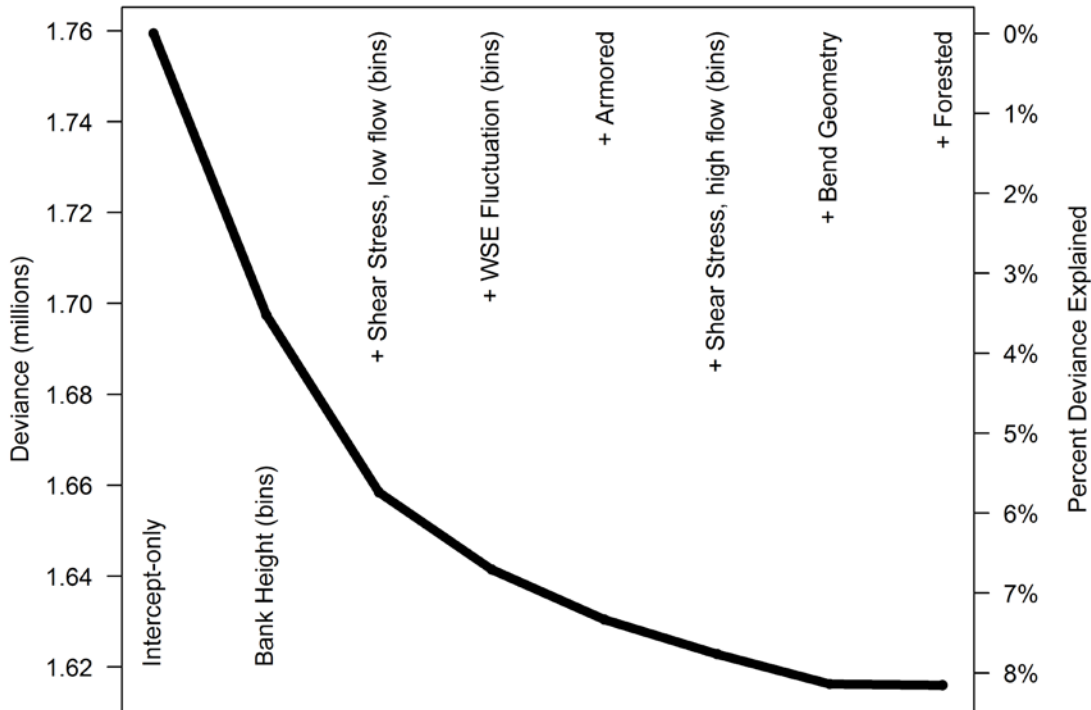


Figure 11. Residual deviance (left) and percent deviance explained (right) for a sequence of logistic regression models adding terms in the order that most diminishes residual deviance; each model includes all of the terms in the model to the left plus the additional term given in each label from left to right. Percent deviance explained is relative to the intercept-only model.

3.2.3 Drilling down for insight

While bank height, WSE fluctuation, and shear stress may rank higher in terms of deviance explained, analysis of armoring and bend geometry as predictors yields some insight. Armoring reduces bank instability: 42.0% of unarmored banks were unstable while only 30.6% of armored banks were unstable. In addition, the outside of bends had lower than average bank instability (35.6%) while inside bends (40.5%) and straight reaches (42.1%) had greater than average bank instability.

There is a greater amount of armor on the outside of bends (24% of banks classified as outside bends were armored compared to 23% for straight reaches and 14% for the inside of bends), but that does not account for the pattern observed. Holding armoring constant, there is less instability on the outside of bends than the other two bend classes. Looking just at unarmored banks, bank instability was 37.8% on the outside of bends compared to 41.1% on the inside of bends, and 45.9% unstable on straight reaches. Looking just at armored banks, bank instability was 28.9% on the outside of bends compared to 36.9% on the inside of bends and 29.6% on straight reaches. Looking at those data from the other perspective, holding bank geometry constant, armoring has its greatest benefit in terms of stabilizing banks on straight reaches and its least benefit on the inside of bends.

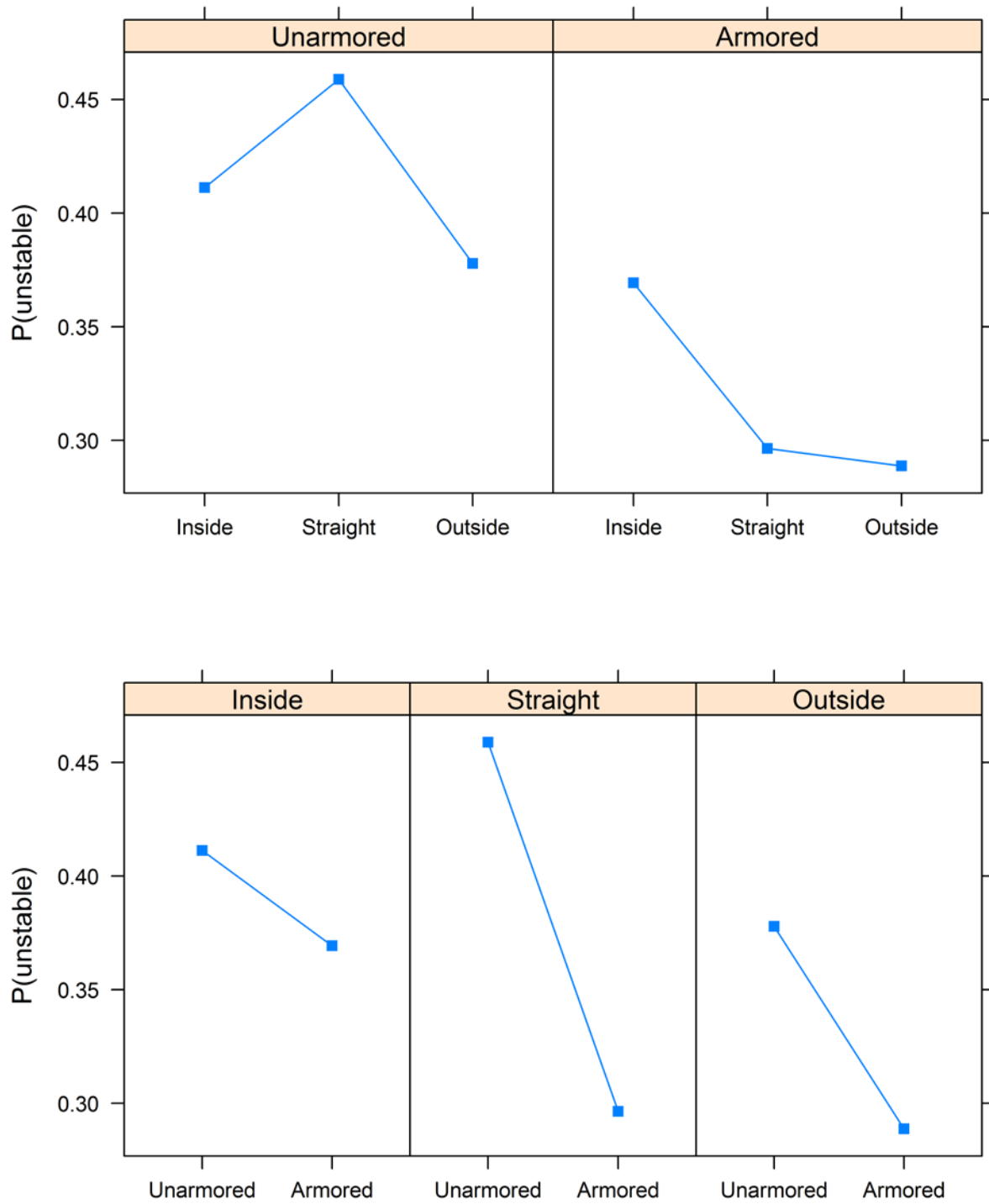


Figure 12. Proportion unstable for unarmored and armored banks on the insides and outsides of bends or on straight reaches.

4. References

- R Core Team (2016). R: A language and environment for statistical computing. R Foundation for Statistical Computing, Vienna, Austria. URL <https://www.R-project.org/>.
- Wood, S.N. (2006) Generalized Additive Models: An Introduction with R. Chapman and Hall/CRC.
- Venables, W. N. & Ripley, B. D. (2002) Modern Applied Statistics with S. Fourth Edition. Springer, New York. ISBN 0-387-95457-0